# Evaluation of CuSCN as a Hole Transport Layer in Flexible Perovskite Solar Cells

A Major Qualifying Project
Submitted to the Faculty of
Worcester Polytechnic Institute
in partial fulfillment of the requirements for the
Degree in Bachelor of Science in
Mechanical Engineering
By

______________________________________
Jason Bugarin

______________________________________
Collin Chen

______________________________________
Jeremiah Leonard

______________________________________
Reese Petersen

Date: 4/26/18
Mechanical Engineering Department
Project Advisor:

______________________________________
Professor Pratap Rao, Advisor

# Abstract

The thin film generation of solar cells is a promising alternative to the market-dominating silicon wafer cells. Thin film cells have the potential for high mechanical flexibility, while having recorded efficiencies that rival that of traditional silicon cells. Hole Transport Layers (HTL) such as P3HT are available for flexible solar cells, but are limited by high cost. Our group aims to determine whether CuSCN, a cheaper HTL, can be utilized to create a flexible solar cell. We compared the power conversion efficiency and mechanical flexibility of cells with CuSCN HTLs to those with much more expensive HTLs. Through this, we discovered that CuSCN can be used to create a working flexible cell but achieves lower efficiency than P3HT and comparable tolerance to bending in thin film solar cells.

# Table of Contents

# List of Figures

# 1.0 Introduction

Harnessing solar energy is a promising alternative to fossil fuels for powering everything from personal electronics to the cities we live in. To increase the use of solar energy, the means by which we harvest the energy must be diversified and improved. The solar industry has been pioneered on rigid silicon solar cells, but with the emergence of solar cells on flexible substrates, we have changed the boundaries of solar energy collection. In an attempt to push commercial flexible solar cell implementation forward, researchers are looking into lowering production costs, increasing efficiencies, and improving mechanical flexibility. The use of both rigid and flexible solar cells could decrease our dependence on fossil fuels by increasing the usability of everyday objects by mounting flexible solar cells to them.

A newer class of solar cells using perovskite structures has been developed and is being looked at as the future of solar cells. These perovskite solar cells have gained attention because of their growing efficiencies, low cost, low processing temperature, and flexibility. In 2014, efficiencies of nearly 20% were reached and researchers continue to increase the efficiencies every year.[1] The use of flexible perovskites would allow for the production of these cells using roll-to-roll processing, therefore significantly dropping costs and allowing for mass production.[2]

There is a variety of different layer combinations that can work as the structure of the solar cell and each material has its pros and cons towards either the processability, the efficiency or the cost of the cell. By testing new materials and interchanging layers in the cell, we can discover new possibilities that will drop the cost of production and could justify the use of less efficient cells by being more economically feasible.

## 1.1 Current Energy Consumption in the US

Humanity has made a staggering amount of technological innovations over recent centuries, making daily life easier and allowing for leisure time. The amount of change in the most recent century alone was a massive leap and human growth is predicted to keep increasing; however, there is one prominent issue with such a projected growth. In order to sustain such a high quality of life in developed countries, there is a massive demand for energy, most coming from fossil fuels, a nonrenewable resource. The First Law of Thermodynamics states that energy is neither created nor destroyed in an isolated system. The Second Law of Thermodynamics states that the entropy in an isolated system can only increase. This means we will always see loss in our conversions of energy, increasing waste, which leads to all the negative side effects of global warming and greenhouse gases. The economic growth of humanity threatens the limited energy resources that exist, which are not renewable and will be depleted. Realistically humanity will not take a step back from the advancements that have been made so rather than remove the use of energy we must make the shift to use renewable sources.

Out of the various resources energy can be obtained from, natural gas and petroleum are the largest contributors. In 2016, the United States consumed roughly 97.5 quadrillion BTU (quads) of energy. In this total, petroleum, natural gas, and coal consumption were tallied at 36.0, 28.4, and 14.2 quads respectively. The combination of these most commonly used fossil fuels is about 78.6 quads, approximately 81% of entire energy consumption in 2016. On the other hand, the total energy consumption through renewable resources was estimated at roughly 11.5 quadrillion BTU, a much smaller 12% of the total 97.5 quads.[3]

Solar energy is one of the least utilized resources in the renewable category. In 2016, the US produced just over 36 billion kWh through solar means, compared to approximately 227 billion kWh and 268 billion kWh through wind and hydroelectric, respectively. Despite its small part of the renewable field it shows the fastest growth rate among renewable sources, from 2010 to 2017, the average cost of solar PV installations has decreased by 70%. During the same period, the total installed solar PV installation capacity in residential applications increased from 250 MWdc to 2250 MWdc, an increase of 900%.[4] When examining the commercial availability of renewable resources, solar is one of the most effective options, as PV cells or arrays can be implemented in any location with sunlight. Solar cells can be placed at any home or business and provide a structure additional electricity generation from a local source, reducing losses from long range electricity transmission.[3]

## 1.2 Solar Cell Energy Collection

The sun is one of the most prominent resources of the earth, as it provides the necessary energy for life to survive and grow. Solar cells, or photovoltaic cells (PV cells), were developed to capture the energy emitted by the sun and convert it into usable energy. While solar collectors can have multiple different applications, the most common use is for electricity generation. By absorbing the sun's radiation, a solar cell is able to generate a current, which is typically fed into the electricity grid.

The primary function of a solar cell is to absorb energy through sunlight. A semiconductor is used as the absorber layer. The nature of the material allows free flow of electrons as energy is introduced to the molecules. There are specific materials that are selected for these layers based on their band gaps, the energy difference between an excited electron and an electron at its low energy state. The band gaps need to be selected properly to ensure an electron will reach a specific energy level.

Once electrons are excited and reach a higher energy state, additional conductor layers are needed to carry the electrons out of the cell. One layer allows the electrons to move away from the original layer, while the other allows the leftover positive charge, or a 'hole' for better visualization, to also move away. The combination of moving electrons and the holes generates the output current that allows for usable electrical power. Since these layers are conductors, the electrical conductivity is crucial to provide sufficient current. One must be careful to factor the change in conductivity as both temperature and shape (and thus cross-sectional area) change, which both vary with different applications of solar cell.

## 1.3 Solar Cell Types

The first prototype solar cells were developed in the 1950s. Since then, three distinct generations of solar cells have emerged, each with a different type of construction and purpose. It is important for the future of solar (and renewable) energy to develop the highest efficiencies while minimizing cost of production and installation. Each generation fulfills a specific need for commercial use and production. Through research and application, there is opportunity to maximize the efficiency of each generation or combine their benefits, but there is room to improve on maximizing the efficiency of each generation or combining their benefits.

The first-generation of solar cells includes cells made of silicon wafers. These cells require a substantial amount of material to manufacture and significant effort to transport and install. The manufacturing process involves creating molten silicon at temperatures in excess of 1400°C in order to form the necessary crystal structure. In addition, the crystalline silicon wafer structure requires the unit as a whole to have a bulky, rigid construction once produced, further complicating transportation and installation. Although they are costly to manufacture and install, and despite being the first to be developed, these cells are still the most common type of solar cell used today. A single junction solar cell with an indirect band gap has a theoretical maximum efficiency of 33.16%.[5] However, typical efficiencies for first-generation cells fall within the 15-25% range.[6]

Second-generation solar cells are categorized as thin film cells. In order to achieve thin films, more amorphous and organic materials are implemented. Though not as efficient as the original crystalline silicon, the organic material layers still allow for reasonable efficiency. With a thin film cell, far less material is required to fabricate the layers and the cell can be annealed in room temperature environments. With shorter processing time and lower material costs, these second-generation cells have the potential to drastically reduce the total cost of solar cell production while only being slightly less efficient than the top of the line first-generation cells.

The most recent generation of cell are called heterojunction cells. This third-generation, although it is the youngest class of solar cells, has already had example prototypes that have achieved efficiencies higher than the theoretical maximum of the previous single junction cells. As more layers (and junctions) are added with different band gaps, it is possible to capture more of the excited electrons. In fact, the maximum theoretical efficiency of a cell with an infinite number of junctions is a staggering 86%.[7]

# 2.0 Background

## 2.1 Perovskite Solar Cell

As solar cells have yet to be the perfect package for a renewable resource, there is still constant ongoing research into new designs. One recent development is the use of a hybrid organic-inorganic absorber layer that has a 'perovskite' structure.[7] The perovskite structure is in the form of $ABX_3$, where A is an organic cation with charge +1, such as Methylammonium (MA), B is a transition metal cation such as $Pb^{2+}$, and X is an anion, typically a halide such as $I^-$.

In solar cells, the perovskite is usually a Methylammonium halide. These types of cells are classified under the second-generation of solar cells, as they are thin film cells. Perovskite solar cells have the capability to be cheaper to manufacture in mass quantities while still achieving efficiencies to rival that of the traditional silicon cells.

One area of interest for these types of solar cells are flexible designs. The desired flexibility is dependent on layer interactions, layer thickness, and the material combinations in solar cells. In addition, the solar cell layers must have a work function profile that works cohesively with the layer design of the solar cell between the absorber and electrode. The most effective work function or conductance band separation between each layer is 0.01eV to 0.03 eV energy difference.[8] This is the optimal energy difference range to move charges between each layer without energy loss from recombination of charges or excess energy release from charges.

### 2.1.1 Substrate

In flexible perovskite solar cells, the most important properties of substrates are the transparency of the material and the flexibility of the material. The substrate is one of the exterior layers that give the solar cell structure, in perovskite solar cells it is usually the layer that allows light to pass through to the inner layers. An essential property in a solar cell is the optical transmittance, which is the amount of visible light allowed through a surface compared to the incident light hitting the surface[9]. The light allowed to pass through a material directly affects the efficiency of the solar cell to power devices. Optical transmittance can be further narrowed in concept to the specific range of wavelengths the material transmits the greatest for solar efficiency. The most important wavelength for solar maximum occurs if the bell curve structure of the transmittance is 500 nm for the visible light range; this wavelength is roughly the middle of the visible light spectrum (400 - 700 nm).[10] The second most dominant property of the substrate is the flexibility of the material that can be described as the bendability of a material. The optimal flexibility as pertains to this research will be on materials with good bendability but low stretching. Our research focused on polyester and polyimides plastics to achieve low cost production and flexible construction. The most common plastics that fit this profile are Polyethylene terephthalate (PET), polybutylene terephthalate (PBT), polyethylene naphthalate(PEN), and polyimide (PI).

PET, a semi-crystalline thermoplastic polyester is a low cost commodity plastic that has a natural color. Polyesters are polymers that have a main backbone structure is formed by esterification condensation of polyfunctional acids and alcohols.[11] These materials have a good strength to weight ratio, good flexibility for various flexible solar cell applications, and the dimensional stability reduces size change due to temperature in the material. This thermoplastic has a high optical transmission about 85% - 90% over the entire visible light range making it a good plastic for transparent applications.[12,13] One positive for using this material in electronics is that it can be commercially bought with an ITO layer deposited on it. ITO is a conductive material commonly used in high efficiency solar cells. This material will be discussed further in Section 2.5.2 Conductor on Substrate. One disadvantage of PET is that the material is a hard plastic rather than a rubber, which means in extreme bending, the material creates creases, which could disrupt conductivity in the cell, and hard plastics in general have a lower cyclic stress life span. Additional key characteristics of the material: it has an inert surface (little reactivity with other materials), the ability to be solution processed and spin coated, and it has strong moisture resistance.[13] These properties of PET have made this plastic a common material used in solar cells and other electrical applications.

Two other polyesters of interest are PEN and PBT. Both polymers are a semi-crystalline thermoplastic polyesters that are similar to PET but have a few advantages and disadvantages. PEN can withstand higher temperatures in processing and long term electrical use which improves electrical applications by increasing polymer degradation but it is also a stiffer polymer.[14,15] PEN has a slightly lower optical transmission at 84% experimentally, but overall the difference is negligible if compared to the transmittance of PET.[15] PBT is a polymer that can be exchanged for PET in many applications to improve flexibility while keeping good strength characteristics.[11] The higher flexibility for PBT could improve flexible solar cell bendability but PBT also has a strong disadvantage of crystallizing at a faster rate.[11] Crystallization will decrease optical transmission of this layer if it occurs in processing of the solar cell and lower solar cell efficiency. Both PEN and PBT have slightly different properties from PET that could be useful or detrimental for different applications.

PI is a synthetic polymer with a high heat and chemical resistance. The plastic has a glass transition temperature at about 260 and a high melting temperature that has not fully studied in literature but it has been determined to be on the order of 400°C, making it a viable material for solar cell constructions that need the layers to be manufactured at high temperature.[16] The material is an optically transparent brown color with a 75% optical transmission(measured with an ITO coating).[16,17] In addition, this material is investigated for use in extreme solar cell and electronics use in general due to favorable radiation resistance, low creep resistance, and electrical insulating ability.[10,18] The high temperature traits of PI identify this material as one of few plastics that can withstand high temperature processing that some commercial and experimental solar cells require. A summary of material properties for all four plastics can be found in Table 1 below.

*Table 1. Plastic Substrate Properties*

| | Material | | | |
|---|---|---|---|---|
| Material Property | PET | PEN | PBT | PI |
| Flexural Modulus (GPa) | 2.758[a] | N/D | 2.63[g] | 4.316[d] |
| Elastic Modulus modulus (GPa) | 3.445[c] | 5.25[i] | 2.5[h] | 3.90[d] |
| Optical Transparence | 87%[b] | ~84%[i] | N/D | >75%[e] |
| Glass Transition Temperature (C ) | 98[c] | 120f | ~78 (estimate)[f] | 260[d] |
| Melting Temperature (C ) | 245[c] | ~265 (estimated) | ~225 (estimate)[f] | >400[e] |
| Cost rank (1-4, 1 is the lowest cost)[f] | 1 or 2 | 3 | 1 or 2 | 4 |

[a] Polyethylene terephalate (PET). Plastic Products INC. Updated 2017. Accessed 10-07-, 2017.

[b] Faraj MG, Ibrahim K, Ali M. PET as a plastic substrate for the flexible optoelectronic applications. J.Optoelectron.Adv.Mater. 2011;5:879-882.

[c.] GEHR plastics PET polyethylene terephthalate.

[d] Ensinger TECASINT 4011 polyimide, yellow (PI). MatWeb Web site

[e.] Lozano A, de Abajo J, de la Campa J, Guillén C, Herrero J, Gutiérrez M. Thin-film polyimide/indium tin oxide composites for photovoltaic applications. Journal of Applied Polymer Science. 2007;103:3491-3497

[F] Polyesters. Polymer Properties Database Web site.

[g] Polyplastic duranex(R) 2002 polyvutylene terephthalate (PBT), standard. Matweb Web site.

[h] Polybutylene terephthalate(PBT) - properties and applications - supplier data by goodfellow. AZO Materials Web site.

[i] Goodfellow polyethylene naphthalate (PEN) film. Matweb Web site.

## 2.1.2 Conductor on Substrate (Anode)

In a perovskite solar cell, the layer above the substrate is a conducting layer that is often called the anode or charge collecting layer. Typically, this layer is designed to be the transparent side of the solar cell so that light can pass through the layer while also conducting electrons that enter the cell. In this layer, it is important that the material being used has both good optical transparency and electrical conductivity. Table 2 below shows important properties for the conductor.

*Table 2. Conductor properties*

| Property | Definition | Desired value for solar cell | Units |
|---|---|---|---|
| Sheet resistance | Measurement of thin film resistance. (Uniform thickness) | Lower sheet resistance is desirable because it reduces the energy lost when collecting a charge | Ohm/cm or Ohm/sq (size independent) |
| Work Function | Energy required to move an electron from the surface of a material | Higher work function is desirable but must also be compatible with the other layers in terms of band gap alignment | eV |
| Band Gap | The electrical distance an electron must travel to reach the conduction band | Should be similar to the band gap of the absorber | eV |
| Optical Transmittance | The amount of light that can pass through a material | A higher transmittance is desirable because it allows more light into the solar cell. | % |
| Fill Factor (FF) | An overall rating of the solar cell's power output that directly relates to its overall efficiency. | A higher fill factor means a more efficient solar cell. | No units: Ranges from 0 - .99 |

### 2.1.2.1 Indium Tin Oxide

Indium Tin Oxide (ITO) is a ceramic that is currently the solar cell industry's premier material for the anode layer of a perovskite cell. This is because it has relatively high optical transmittance, depending on its thickness, while also having a very small sheet resistance of 50-60 ohms/sq.[19] ITO has superior conductance compared to the alternatives for the anode but it also possess two major drawbacks, cost and brittleness. Indium is a rare element that it is in high demand and as a result it is very expensive. It has been found that ITO's brittleness may cause a drastic decrease in its ability to conduct. In a cyclic bend test done on a ITO/PET based solar cell, crack formation was attributed to ITO's brittleness.[20]

### 2.1.2.2 Carbon Based Conductors

As an alternative to ITO, many researchers have looked into using carbon-based conductors like graphene and carbon Nanotubes (CNTs). Graphene sheets are being used in the anode layer mainly because of their superior flexibility and transmittance of nearly 97%.[21] One of the drawbacks of graphene is that multiple layers are needed to increase the conductivity because of its high sheet resistance of 225.7 ohm/sq.[22] One other problem with graphene sheets is that they are extremely hydrophobic, so coating the hole transport layer on top of it can be very difficult.[16]

CNTs are similar to graphene in that they are very flexible but their high electrical conductivity of 2000 S/cm sets them apart from graphene sheets.[23] These carbon Nanotubes exhibit great mechanical and electrical properties as individual tubes but when but in large arrays like films, these properties degrade drastically. This problem is due to a series of factors but all stem from the junction resistance created between the CNTs in the array.[16]

### 2.1.2.3 Nanowire Arrays

Nanowires (NWs) have gained increased attention over recent years as a novelty conducting layer of a flexible solar cell. The most common NW arrays are made up of silver and gold, due to their high work functions, but copper NWs have also been looked at for cost reduction.[24] The NWs, like CNTs, have lower transmittance than other anodes because they are inherently not transparent but allow light to pass through in array gaps. However, both transmittance and sheet resistance can be enhanced by manipulating different arrangements of wires, combining wires with other materials and identifying the ideal dimensions of the wires. Various studies have demonstrated that longer and thinner wires are ideal for these properties.[25-27]

A paper in 2010 conducted a study that attempted to show how Ag NWs compared to ITO as an anode layer. They grew Nanowires of various diameters and lengths to identify and therefore optimize the NW arrays sheet resistance and transmittance. They ultimately decided to use NWs with a diameter of 30 nm and a length of 30 µm. The Ag NW electrode they made produced excellent results with a transmittance of 80% and a sheet resistance of 20 ohm/sq.[26]

Although, these NWs seem to be superior to the other anodes, it is important recognize their areas of weakness. Ag NW's are especially difficult to use in perovskite solar cells because they have shown to undergo degradation when in contact with halogen ions.[28] The NWs have also shown to be sensitive to heat which could lower their overall efficiency.[29] Finally, from the research done on NW's it has been seen that the procedure can be complicated and expensive because of the use of Ag and Au.

Table 3 summarizes the characteristics of several of the most popular organic solar cell conductor layers though the work function column was limited by the availability of the information. This information was pulled from the sources listed in the section above, which focused on the conductors in the cell.

*Table 3. Conductor Comparison*

| Material | Sheet Resistance | Optical Transmittance | Work Function | Electrical Conductivity |
|---|---|---|---|---|
| ITO[a] | 50-60 ohm/sq | 90% | | 1000 S/cm (CNT thin) |

| | | | | |
|---|---|---|---|---|
| Graphene Sheets[b] | 225.7 ± 6.0 ohm/sq | 97% | 4.4 ev (Diodes) | 500 S/cm (CNT thin) |
| Carbon Nanotubes[c] | 150 ohm/sq (CNT thin) | 80% | | 2000 S/cm (CNT thin) |
| Ag Nanowires[d] | 15-60 ohm/sq | <56 % | | 45454 S/cm (CNT thin) |

[a] Sigma Aldrich

[b] Efficient Flexible Organic/Inorganic Hybrid Perovskite Light-Emitting Diodes Based on Graphene Anode Seo, Kim, Lee and 7 more. (2017) - Advanced Materials, 29 (12)

[c] Carbon Nanotube Thin Films: Fabrication, Properties, and Applications

[d] Scalable Coating and Properties of Transparent, Flexible, Silver Nanowire Electrodes Hu, Kim, Lee and 2 more. (2010) - ACS Nano, 4 (5), 2955-2963

### 2.1.3 Electron Transport Layer

The purpose of the electron transport layer is to allow movement of the excited electrons to a conductor layer. In a perovskite solar cell, this layer allows the electrons to travel from the perovskite absorber to the conductor, which will allow the electrons to flow away and generate current alongside the hole movement. Typical selections for this layer are metal oxides. These are very efficient at allowing the electrons through to the corresponding conductor.

In a flexible solar cell, materials need to be carefully selected to ensure proper flexibility while maintaining efficiency. Typical options for this layer are metal oxides, which act as excellent semiconductors. A common example is titanium oxide. However, because it is a metal material, it requires an annealing or sintering process to be formed onto the solar cell. Temperatures required for such processes reach values too high for a solar cell to remain flexible after processing. In most cases, the temperatures will simply melt the cell, as the thin film cells are primarily made up of organic and amorphous materials. However, newly developed processes have allowed zinc oxide, ZnO, to be added to the cell without annealing.[30] There are several different methods to achieve this, but the most common answer was to undergo a solution based process. By dissolving zinc acetate in methanol, the result is a solution of ZnO that can be added onto the conductor.[31]

There are several factors that make zinc oxide an excellent choice for this solar cell over titanium oxide, a popular choice for the electron transport layer. While ZnO and $TiO_2$ have similar energy band gaps, ZnO has a much higher electron mobility, allowing more electrons to easily pass from the absorber to the conductor and improving efficiency. It also has a slightly lower refractive index, allowing for a less opaque cell if all transparent layers are required or specified (see Table 4 below).[32] The thickness of the layer must also be considered, as different thicknesses will affect current density and efficiency. In practice, ZnO Nanoparticles in a MAI perovskite solar cell has an ideal thickness of 25 nm, as shown in Table 5. A ZnO layer also has a band gap of -4.2 eV to -7.5 eV, making it an ideal candidate when paired with the adjacent perovskite absorber layer and the adjacent conductor.[31]

*Table 4. Electron Transport Layer Properties*[32]

| | ZnO | $TiO_2$ |
|---|---|---|
| Crystal Structure | Rocksalt, zinc blende, wurtzite | rutile , anatase, and brookite |
| Energy Band Gap (eV) | 3.2-3.3 | 3.0-3.2 |
| Electron mobility ($cm^2\ V\ s^{-1}$) | 205-300 (bulk), 1000 (single Nanowire) | 0.1-4 |
| Refractive Index | 2.0 | 2.5 |

*Table 5. Thickness Variation of ZnO*

| Device parameters for solar cells prepared with varying thickness of ZnO[a] | | | |
|---|---|---|---|
| No. of layers | ZnO thickness (nm) | J (mA/cm^2) | PCE (%) |
| 0 | 0 | 16.5 | 2.4 |
| 1 | 10 | 18.0 | 11.1 |
| 3 | 25 | 20.5 | 14.4 |
| 5 | 40 | 18.9 | 13.3 |
| 8 | 70 | 18.4 | 12.9 |

[a] Liu D, Kelly TL. Perovskite solar cells with a planar heterojunction structure prepared using room-temperature solution processing techniques. Nat Photon. 2014;8(2):133-138.

## 2.1.4 Absorber

The most important layer in a solar cell is the absorber; it allows photons entering the solar cell to create electrical current. When photons interact with a semiconductor within a solar cell they cause loosely held electrons to move into an excited state forming holes at the same time. Each time a photon hits the material the wavelength of light absorbed will determine how excited the electron is. An electron will leave its valence bond for the conductor band if it receives an excitation voltage within a specific energy range. This electrical energy is called the band gap and for a single absorber solar cell there is a limit to the efficiency of any solar cell directly related to the band gap called the Shockley Queisser Limit.[33] This limit incorporates all the losses of energy in the transfer of electrons within a single layer cell and calculates a max theoretical efficiency of 33.7% with a band gap of 1.34eV.[34] This is shown below in Figure 1.

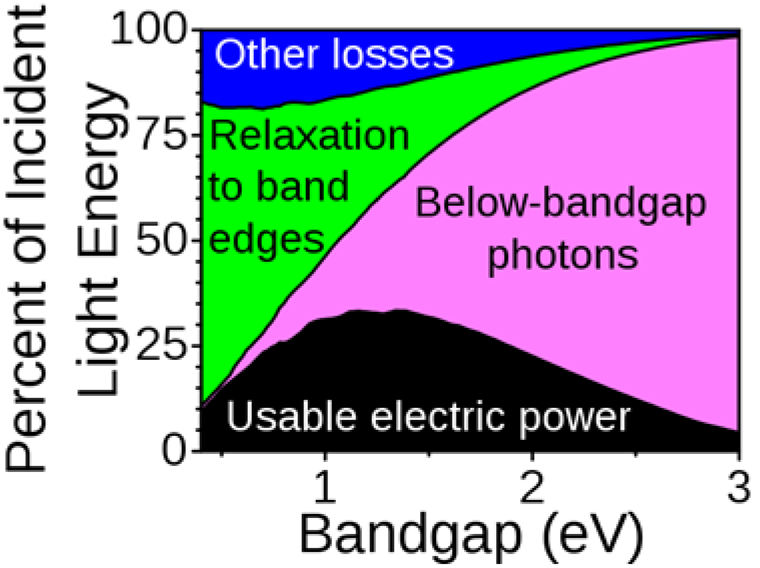

*Figure 1. Shockley-Queisser efficiency explanation.*[35]

### 2.1.4.1 Perovskites

A perovskite absorber solar cell shows some of the greatest promise in the advancing solar cell field. They are extremely lightweight in comparison to Silicon and because of the ease of production costs can be kept reasonably low. Perovskites have risen in efficiency as well, with the maximum PCE of cells going from 3.8% to 22.1% in just seven years.[36]

Even with perovskite cells becoming so promising, they still have several drawbacks with stability that could affect their potential for silicon cell replacements. The most significant is that the cells suffer from fast degradation in the presence of oxygen or moisture.[37] This is due to the water solubility and easy oxidation that comes with parts of the cell being organic. Because the organic nature is vital to the success of the cell that cannot be changed; however, by improving the sealing and effectively weatherproofing the cell during fabrication you can prevent immediate degradation of the cell due to moisture.[38]

A second major limitation to Perovskite cells is their use with $TiO_2$ as an ETL. While $TiO_2$ is an effective ETL, the layers react to ultraviolet light the $TiO_2$ present in the cell causes efficiencies to decrease.[39] While there has been the correlation made that $TiO_2$ is the perpetrator to the loss of efficiency it's not yet clear specifically how the UV light affects the solar cell stability.

### 2.1.4.2 Methylammonium Lead Iodide ($MAPbI_3$)

Methylammonium lead iodide ($MAPbI_3$) has a band gap of 1.51 eV, and an efficiency limit of around 31.5%, which puts it on a very competitive scale with silicon based cells which have a theoretical maximum of 32.2%.[5,40] It's also similar to silicon in terms of free carriers in the excited state and an almost perfect crystalline film formation containing minimal defects.[41,42] MAPbI$_3$ challenges the silicon standards but still has a major drawback of being volatile in open air to humidity degradation. While there is the benefit that the cells can be produced at low temperatures, a secondary drawback is their instability at higher ranges. Cells can start to show degradation at temperatures as low as 85°C which can severely limit potential applications.[43] The composition is also reliant on lead, which is seen as a limitation to commercialization, though there have been investigations into replacing lead with Tin or Bismuth among other elements.[44]

### 2.1.4.3 Formamidinium Lead Iodide (FAPbI$_3$)

Formamidinium lead Iodide (FAPbI$_3$) has a band gap slightly narrower than that of MAPbI$_3$ at 1.48 eV which is comparable and has the potential to make FAPbI$_3$ a likely substitute for MAPbI$_3$ as the cation of the perovskite grouping.[45] There are multiple phases of the FAPbI$_3$ solution, the phase most conducive to the functioning of a solar cell is the dark α-phase which is only stable at temperatures above 160°C. Powdered versions of the different FAPbI$_3$ phases are shown below in Figure 2. In an ambient humid environment this is observed to change into the non-perovskite δ-phase and poses a challenge to creating and maintaining a functioning cell. This has been combated by adding in stabilizing chemicals such as MAPbBr during solar cell fabrication.[46] The humidity in particular poses a great challenge as cells that had been created in a 2% humid environment had PCEs of 16.6% but when created in a 40% humid environment had PCE around 8.6%.[47]

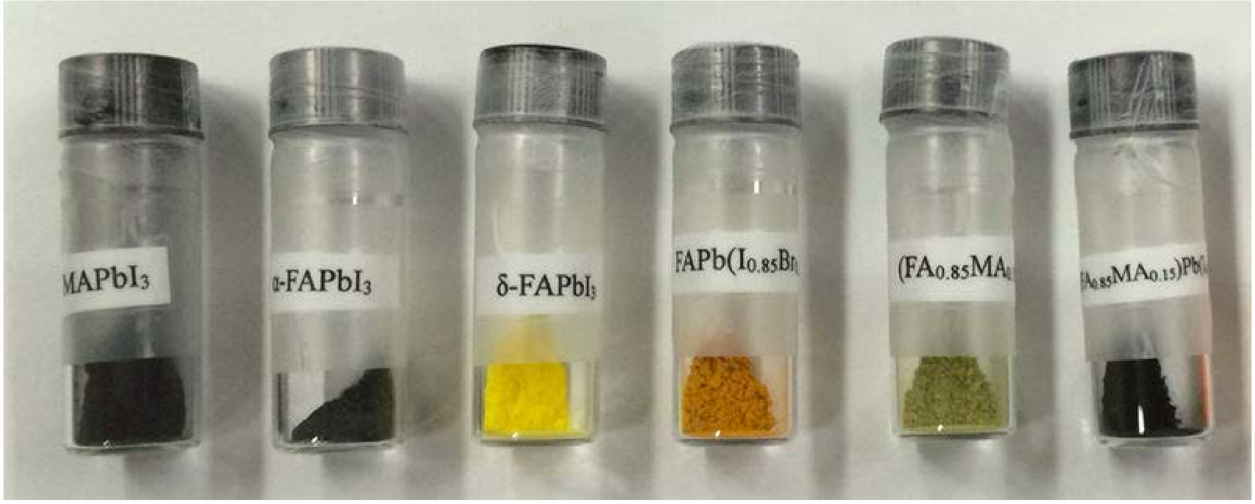

*Figure 2. The different forms of FAPbI$_3$.[46]*

## 2.1.5 Hole transport Layer

The Hole Transport Layer (HTL) controls the positive charge movement in the solar cell from the absorber to the conductor. The most important features of the HTL is to be flexible, have strong hole mobility, and have a work function that is efficient with the absorber and electrode next to the HTL. Hole mobility is the rate of a single positive change moving in a given volume.[8] Higher values for hole mobility move charges from the absorber to the conductor faster resulting in higher efficiencies of the cell to the electrical storage. The flexibility of this layer is important so the layer can take enough strain repeatedly in bending to be used as a flexible solar cell component. In our research the most common materials used for flexible solar cell HTL layers were the organic compounds poly(3,4-ethylenedioxythiophene)–poly(styrenesulfonate) (PEDOT:PSS) and 2,2′,7,7′-tetrakis(N,N-di(4-methoxyphenyl)amino)-9,9′-spirobifluorene(Spiro-MeOTAD). One material of high interest is copper thiocyanate (CuSCN), a material being researched in non-flexible solar cell applications because of its good charge conducting properties.[48]

PEDOT:PSS has good flexibility, good processability, and the ability to have properties altered with additives. The combination of high optical transmission greater than 80% and the ability to create thin film layers has made PEDOT:PSS a common HTL.[49] PEDOT:PSS has good layer surface coverage of 95% to yield even thin layers and it has controllable conductivity to aid charge movement.[50] The conductivity and surface coverage maintains good efficiency of the cell and limits any issues of short-circuiting from layer contacts through the HTL layer. One weak point of PEDOT:PSS is that the layer is not a sufficient electron-blocking material without [51] additives to the layer.[48] In addition, the use of PEDOT:PSS is limited by the nature of the material being acidic which can increase degradation in some absorbers and metal oxide layers, but specific ETL layers have been found that are not degraded by this material (ZnO and TiOx).[49] As long as PEDOT:PSS is used with materials that are resistant to its acidic nature it has exhibited good hole transport behavior in solar cells based on its ease of processing thin full coverage films.

Spiro-MeoTAD has similar properties in comparison to PEDOT:PSS such as work function and good flexibility. The hole mobility for Spiro MeOTAD about 4.0e-5 $cm^2V^{-1}S^{-1}$ and is one of the highest hole mobilities for organic compounds.[52] In literature, exact surface coverage values and optical transmission were not found for this material but the processability to make even layers and the high optical transmittance is similar to PEDOT:PSS. One advantage that Spiro-MeOTAD has is that it has a higher solubility, allowing the material to be more easily coated between Nanoarchitecture.[53] This has been a reason for research with Spiro MeOTAD as an HTL to test different surface finishes and solar cell layer constructions. This organic HTL material is an efficient hole transport layer but it has decreased in use compared to PEDOT:PSS due to a higher price with similar properties between both organic compounds.

P3HT or Poly(3-hexylthiophene-2,5-diyl) is a semiconducting plastic with a high hole mobility of 0.12 $cm^2V^{-1}S^{-1}$ making it an ideal hole transport layer in organic solar cells. In addition to this, the layer is easily soluble and is relatively stable in air. Because of P3HT's versatility as a hole transport it is often the choice comparison for any new materials that work as a p-type layer. The main drawback for much of the uses of P3HT is its cost of production and use, which can be extremely high at almost $400 per gram.[54]

One material in preliminary research in solar cells, CuSCN, could drastically improve the charge transport if applied to flexible solar cells. CuSCN is a pseudohalide, which consists of singly ionized copper and a thiocyanate group.[55] The ratio of anions to cations in this material is based on the deficiency of copper cations; the larger the deficiency of copper ions, the larger the hole mobility in the material.[56] CuSCN is an interesting material for flexible solar cell applications because it does not cost as much as organic HTL layers and the hole mobility is significantly greater at 0.1 $cm^2V^{-1}S^{-1}$ to organic compounds.[52] CuSCN also has a high optical transparency being 98% in the 390-750 nm wavelengths and 89% in the 400-1300 nm wavelengths.[55] The work function of CuSCN aligns well to the perovskite absorber with only a 0.1 eV difference and it has a large band gap that limits ability of electrons to travel around CuSCN to the opposite conductor.[55] The main disadvantage for CuSCN is the brittle nature the pseudohalide could introduce to the perovskite solar cell. The flexible nature of the solar cell could be limited in comparison to the plastic HTL layers currently used in flexible solar cells. If CuSCN solar cells have a good efficiency to flexibility ratio for certain applications, this construction could be advantageous. Another consideration is that CuSCN has shown interdiffusion between perovskite absorbers; considerations would have to be made to limit this interface diffusion in processing.[55] Overall, CuSCN has many interesting properties that could be a great HTL for perovskite solar cells and extensive experiments with this material will be the only way to understand its limits in perovskite flexible solar cell technology.

Table 6 summarizes the properties of the Hole Transport Layers that are most common in flexible organic cells for easy comparison.

*Table 6. HTL Properties*

| | Material | | |
|---|---|---|---|
| Material Property | PEDOT:PSS | Spiro-MeOTAD | CuSCN |
| Hole Mobility (cm^2V-1S-1) | <4.0e-5 | 4.0e-5[b] | 0.1[a] |
| Work function(eV) | 5.2[d] | 5.2[c] | 5.3[a] |
| Optical Transparency | 80%[f] | 80%-85% (estimated) | 98%[e] |

[a]Peng Q, Tanaka S, Ito S, et al.  inorganic hole conductor-based lead halide perovskite solar cells with 12.4% conversion efficiency. Nature Communications. 2014.

[b] Lee SJ, Pil Kim H, Mohd Yusoff, Abd Rashid bin, Jang J. Organic photovoltaic with PEDOT:PSS and V2O5 mixture as hole transport layer. Solar Energy Materials and Solar Cells. 2014;120(Part A):238-243.
[c] Zhou H, Chen Q, Li G, et al. Interface engineering of highly efficient perovskite solar cells. Science. 2014;345(6196):542-546.
[d] Docampo P, Ball JM, Darwich M, Eperon GE, Snaith HJ. Efficient organometal trihalide perovskite planar-heterojunction solar cells on flexible polymer substrates. Nature Communications. 2013;4.
[e] Wijeyasinghe N, Anthopoulos TD. Copper(I) thiocyanate (CuSCN) as a hole-transport material for large-area opto/electronics. Semicond Sci Technol. 2015;30(10):104002.
[f] Lattante S. Electronics. Electronics. 2014;3(1):132-164.

### 2.1.6 Conductor (Cathode)

The final layer of a perovskite solar cell is another conducting layer often called the cathode layer. This layer is typically not transparent because it is not the side of cell where light comes through. Its only job is to conduct the electrons that are captured in the cell and keep them flowing to complete the circuit. All of the anode layer options can be used in the cathode layer, essentially making the cell fully transparent, but more often a thin metal film is used to offer greater conducting ability. The metals used for this layer are usually high work function noble metals like gold, silver and nickel.[57] Work function and cost are the two driving factors in selecting a material for the cathode layer. Table 7 displays several conducting materials and their work functions.

*Table 7. Work Functions*

| Metal | Gold | Silver | Nickel | Platinum | Copper | Chromium |
|---|---|---|---|---|---|---|
| Work Function (ev) | 5.32 | 4.64 | 5.15 | 5.4 | 4.7 | 4.4 |

Ahn J, Hwang H, Jeong S, Moon J. Metal-Nanowire-electrode-based perovskite solar cells: Challenging issues and new opportunities. *Adv Energy Mater*. 2017;7(15).

## 2.2 Fabrication Methods

A large factor contributing to the costs of solar cell production lies directly within the production techniques themselves. Silicon cells require extensive amounts of processing and extremely high temperatures. The processes to meet the energy demand of roughly 90% of commercial solar cells being silicon have increased in magnitude and become streamlined; however, they are still limited by those production costs.[58] Organic solar cells as well as having promising efficiency potentials are paralleled by the cheap production options and processing techniques encompassed by roll to roll processing.

### 2.2.1 Roll to Roll Processing

Roll to Roll (R2R) is an over encompassing title for several more specific processes, and is the ability to manufacture product using flexible substrates and create continuous product production. The immediate benefits of this process are the streamlined methods that do not require excessive labor or even necessarily the transfer of material from one process to another. There are several specific methods that can be placed one after another in R2R manufacturing line to complete a final product.[59]

#### 2.2.1.1 Chemical Vapor Deposition

Chemical Vapor Deposition, or CVD, is a chemical process that causes volatile precursors in the gas phase to form a solid layer on the target surface. Generally, CVD takes place at low pressures because the particles being deposited tend to exists as liquids in normal conditions. The conventional method of CVD is thermally activated CVD, which causes the chemical reaction to happen by a change in temperature. Another common method is Photo-initiated CVD, which triggers the deposition by the addition of light, usually UV causing the monomers to layer on the substrate.[60]

#### 2.2.1.2 Physical Vapor Deposition

Very similar in principle to CVD, Physical Vapor Deposition (PVD) relies more on physical interactions than chemical ones. Like CVD there are subsets of PVD, Sputter Deposition specifically is the ejection of particles into a vacuum chamber. Particles are usually ejected by a continuous flow of argon gas. The particles being sent into the vacuum are subject to a negative potential while the target substrate is grounded; this leads the ejected particles to evenly coat the substrate in a very thin layer of a conductive material. PVD coatings offer the benefits of improved hardness and oxidation resistance as well as a smooth layer, which is most beneficial for the solar cell process.[61]

#### 2.2.1.3 Solution Based Processing

As suggested by the name this process involves creating a solution with the desired material dissolved into a soluble substance. That solution is then spread onto the surface where the layer is to be coated to a desired thickness; the solution is then either treated or heated to evaporate the processing solvent. This method can be paired with spin coating to achieve a desired thickness of a material; however, spin coating is not conducive to R2R processing.[62]

### 2.2.1.4 Doctor Blading

Doctor Blading is a process common to R2R where the substrate and a deposited solvent are either dragged under, or held while a blade drags over. The blade is at a fixed distance from the material the solvent is added to, this distance determines the thickness of the doctor bladed layer. In R2R setups on a larger scale the doctor blade is at a set distance from a large cylinder where the flexible substrate and solvent are passed, the blade removes excess solvent leaving a thin film. Common for lab practices is the second technique where the substrate has two very thin buffers attached with a gap in between. The solvent is placed in the gap and the doctor blade is pulled along the buffers, leaving a film the thickness of whatever was used as a buffer.[63,64]

### 2.2.1.5 Sol Gel Process (ZnO)

Sol Gel processing is a common method for synthesizing Nanoparticles because it can be done at low temperatures compared to other methods. At a chemical level, the process involves reacting a base material with another solution over a specific amount of time to produce a sol, a solution with suspended Nanoparticles. The addition of the secondary solution relies on the use of a titrator to accurately “drip” the solution into the other over a calculated time. The sol gel process relies on specific stoichiometric principles to produce these Nanoparticles. ZnO particles are a common example of a sol that is produced via sol gel processing. [65]

### 2.2.2 Spin Coating

When depositing a thin film onto a substrate especially in a laboratory setting spin coating is often used because of its benefits in uniformity. This application method uses centrifugal forces on a disk spinning at high speeds to create an even coating on a substrate. The layer thickness is heavily dependent on viscosity, speed of the spinner, and the time the material is allowed to spin for.[66] There have also been applications of spin coating that use gas assisted methods which have been shown to produce smoother crystallization and reduce drying time of a substance onto the substrate.[64] A downside of using spin coating is that much of the material is wasted, leaving only 10% of the solution utilized.[67] It is also very impractical for large scale manufacturing.

## 2.3 Mechanical testing

Inorganic-organic perovskite cells have had limited mechanical testing in comparison to organic flexible plastic solar cells. Research in flexibility and deeper analysis of failure in perovskite solar cells could increase the understanding of the mechanisms of failure and create limits of applications for specific material being investigated. The solar cells are created with up to five interacting layers in a single junction solar cell that must have good layer coating, layer adhesion to one another, and similar material properties to work in a variety of conditions. Differences in thermal expansion, the stiffness of the material layers, and interface interactions can limit the mechanical deformation of the solar cell and even short the electric circuit. This knowledge could help make perovskite solar cells increase efficiency to match silicon solar cells. To analyze trends in failure of solar cells, a variety of testing to record measurements can be employed; these areas could be in bend testing, adhesion testing, tensile testing, and compression testing.

First, bend testing is one of the most common tests done on flexible solar cells due to bendability/flexibility being one of the greatest features of these devices. The tests are engineered to be 1-dimensional tests to only test changing parameters in one direction. The types of bend tests used are either bend tests to failure of the solar cell or cyclic bend tests of a specific radius of curvature. Cyclic bend tests can test the materials stability under deformation for an extended period of time on different bends to signify the durability of a material.[68] The test of layer failure consists of choosing a bend radius and measuring the resistance change over bending cycles to the chosen radii, at the drop of resistance, the test was stopped and SEM images were taken.[68] For bend tests, a plastic system or a metal clamp system is used with the solar cell held on one side for a simple support or the cell is clamped on both sides for clamped end tests.[69] These devices are measured for output current vs input voltage over the mechanical testing to indicate when the solar cell fails or begins to lose efficiency. Tests of this nature are done instead of three or four point bend tests due to the extreme flexibility of the devices, because such tests do not incorporate sufficient bending to cause failure in the solar cells.[69] Bend test data is important to consider because bending is the most common distortion for thin film solar cells in typical applications. Bend tests have the ability to be focused on individual layers and interfaces to determine the bending limit of each layer to make further material characterizations than can be done with testing the entire cell.

Compression and tensile testing are used in flexible solar cells to identify additional failure mechanisms that can arise in product use not related to bending. Most tests are engineered to be 1-D tests to only test changing parameters in one direction. At times, biaxial compression and tension tests are used to test extreme forces of tension or compression under the same test conditions.[70] The types of compression/tension tests used are either tests to failure of the solar cell or cyclic tests of a specific compression/tension percentage or distance. The same premise of each type is the same as in bend testing described in the previous paragraph. The test systems used are plastic or metal spacers that sit 1 cm larger than the sample and the sample sits on a pre-stretched elastomer or similar material that can move with the spacers.[70] The solar cell sticks to the stretched elastomer to keep the cell in place in the compression test and tensile tests. In both tests, the spacing is increased or decreased slowly in consistent intervals that relate to specific percentages of compression or tension and the test stops when the solar cell fails to convert energy.[70,71] Tensile and compression distortions during application use are less likely but will yield important information on forces placed on the solar cell that could decrease the life of the solar cell.

Alternatively, the test can be done in a cyclic test to gain information on durability of the solar cell in a similar regard to cyclic bending testing.[70] Cyclic stretching is another test method that is similar to tension and compression testing but this test creates both types of stress. These tests will use similar test setups and procedures as the tension and compression tests, the difference is these tests will have a specific tension/compression percentage that will be repeated in each stress mode until solar cell failure.[70] This test is useful to test how multiple forces could change the failure rate of the material and if the failure is of a different mechanism.

Lastly, peel testing can be used on flexible solar cells to test the adhesion/cohesion forces between the solar cell layers. This testing technique can determine the limiting interface and the energy required to causes delamination.[72] Peel testing on flexible solar cells is done in a double cantilever beam method by epoxy bonding two elastic beams to the solar cell on opposite sides.[72] The load and displacement changes are recorded to identify the force needed to fracture the solar cell. This measurement can be then further analyzed by SEM images to characterize the fracture surface. This mechanical test method can give quantitative and qualitative data for the weakest layers in the solar cell to identify the limiting interface. The tests can also be done on individual interfaces to estimate the adhesion strength between each layer. Pull testing could obtain specific data for each layer to analyze the effect each material has on the solar cell.

## 3.0 Scope

This project aimed to evaluate the use of CuSCN as a HTL in a flexible solar cell. CuSCN solar cells has been found to reach efficiencies similar to P3HT but its flexibility has not yet been extensively tested. The solar cell was constructed from bottom up according to Figure 3.

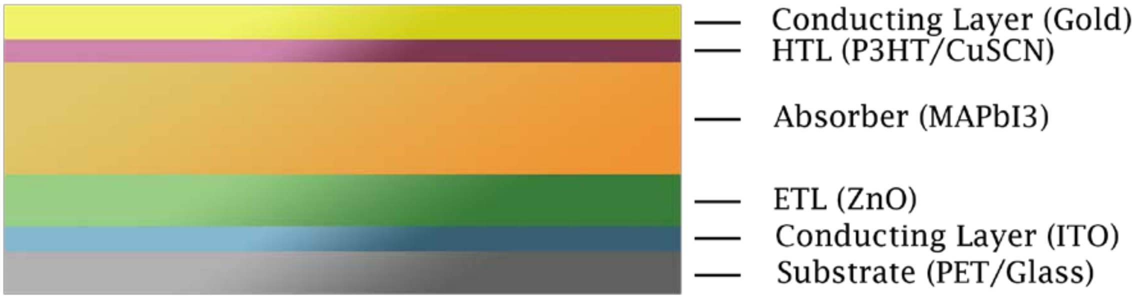

*Figure 3. Layout of solar cell structures.*

To fabricate these solar cells we attempted to follow the overall methods of Liu, D. and Kelly, T.L., 2014 with supplementary additional research papers that used similar layers, and processes that were suitable for our lab and on plastic substrates.[31] It was quickly discovered that the procedures presented in these papers were often vague and required strong background knowledge of solar cell fabrication. To produce a successful and repeatable procedure for our cells we had to perform extensive investigative experiments for each layer. Through the fabrication of various solar cell iterations, we developed an improved and in depth procedure for producing each layer of our cells. We conducted Power Conversion Efficiency (PCE) tests to determine efficiency comparisons between the two types of cells. To evaluate flexibility performance, we bent different kinds of cells around varying radii and measured resistance changes to help evaluate potential layer separation. This layer separation could drastically lower efficiencies by increasing electrical resistance, disrupting the flow of charges in the cell. To determine CuSCN's flexibility we compared it to P3HT under the same bending conditions.

# 4.0 Methods

The fabrication of the solar cell required building upon and modifying several methods found in research to the materials and lab tools available. The following section will delve into the final processing that was used to formulate each solution and resulting solar cell layer. The cells were also subsequently tested mechanically to establish comparisons in layer longevity between CuSCN and P3HT and their effects on inter-cell layer bonding. To summarize the materials used for the solar cells, a table has been placed in Appendix C “14.1 Chemical List” for reference in conjunction with our materials processing methods that will follow in this chapter.

## 4.1 Substrate & Indium Tin Oxide Layer

The solar cells were tested on two different substrates, ITO coated glass and ITO coated PET. ITO is the solar cell’s electron conductor layer, which was layered on top of the substrate base to give the cell its rigidity or flexibility. Both glass and PET were obtained pre-coated with ITO to help minimize the total fabrication time and possibility for errors. Before flexible tests were to be considered, it was important to make sure the entire cell could be fabricated and could function. These first iterations of the solar cells were carried out using glass as the substrate. Glass allowed for easier handling and SEM imaging of the cell while the rest of the solar cell layers were studied and optimized. Once each processing method was finalized, tests were carried out on PET to meet the goal of developing a flexible unit.

Each sample was cut to a size of 20mm by 25mm, which allowed space for multiple solar cells and enough excess material for SEM imaging. The glass samples were scored using a diamond stylus and cracked with glass running pliers while the PET samples were cut using either a razor or scissors. Despite being obtained in new sheets from a supplier, all substrate materials were cleaned after cutting to size. Samples were rinsed in a 1:1:1 solution of water, acetone, and isopropanol before being placed in a sonic vibrator cleaner for five minutes, this was then repeated two more times. A final step was taken by rinsing the samples in a 1-propanal solution before sonication for 20 minutes.

To prevent short-circuiting between the top gold conductor and the bottom ITO of the final cell was etched away. Kapton tape was used to cover the entire ITO surface except a 5-7 mm space on the 25 mm side of the glass slide. Zinc powder was lightly spread across the unmasked ITO, and hydrochloric acid (HCL) was slowly dropped on to react the zinc. During the reaction, ITO is removed from the unprotected substrate leaving just the substrate. The remnants of the HCL and zinc reactions were washed away with deionized water. After removing the masking Kapton tape, the previously described cleaning method was then followed several times in order to clean the cells before adding the ETL. In Figure 4 examples of the etching process and the difference of ITO etch glass. Detailed procedures can be found in Appendix A “12.1 Substrate Etching and Cleaning Procedure”.

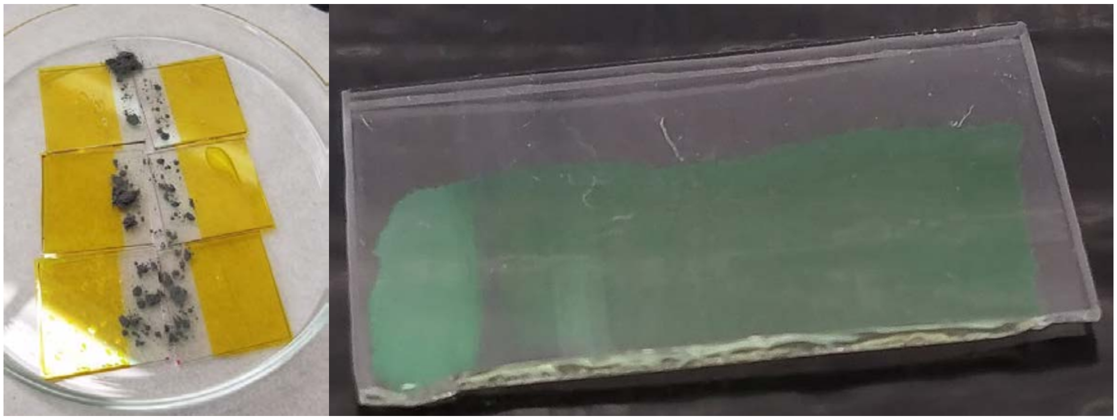

*Figure 4. (Left) Unetched ITO glass with Kapton tape and Zinc powder. (Right) ITO on glass after etching.*

## 4.2 Zinc Oxide Nanoparticles Layer

The electron transport layer of our cell is comprised of a thin layer of ZnO Nanoparticles. This layer was initially synthesized as a solution using sol gel processing that is spun coat onto the ITO layer following the Liu, D. and Kelly, T.L., 2014 process.[31] Zinc acetate dihydrate was combined with methanol in a 13.4 mmol solution which is stirred and heated at 65°C. A second solution of potassium hydroxide (KOH) in methanol was made with a 23 mmol concentration. The KOH solution was added dropwise to the first solution over a period of 15 minutes. The now combined solution is left to stir for 2.5 hours at 65°C then allowed to cool for an hour which lets formed precipitates separate enough from the liquid to partially decant. A centrifuge was used to separate the particles further, which are then washed and mixed in a methanol solution. The centrifugation and washing steps are repeated 3-4 times to fully clean the ZnO particles. A mixture of 35 ml n-butanol, 2.5 ml methanol and 2.5 ml chloroform is mixed and the Nanoparticles are added. To help get the Nanoparticles out of the centrifuge containers, the solution is swished in with the particles and, when necessary, a clean glass stir rod was used to remove the precipitated particles.

Once prepared, the solution was sonicated for 20 minutes before it is spin coated to break up and suspend the particles evenly in the solution. Once suspended, the whole solution was filtered using 25 µm filter paper which can be stored in a beaker with a parafilm covering. Before spin coating, the solution is sonicated for at least 5 minutes filtered through the 0.45 µm PVDF syringe filters to remove the remaining large particulates. The solution was spun coat onto a ITO coated substrate at 3000 RPM, 30 seconds of spin time and an acceleration 1000 RPM/s. This coating is repeated 5 times per sample to get a coating thickness between 90 and 120 µm. The last step is to wipe plain glass region of the ZnO layer. A sample of ZnO can be viewed in Figure 5 below. The complete procedure for this layer can be found in Appendix A "12.2 Zinc Oxide Nanoparticle Layer Procedure"

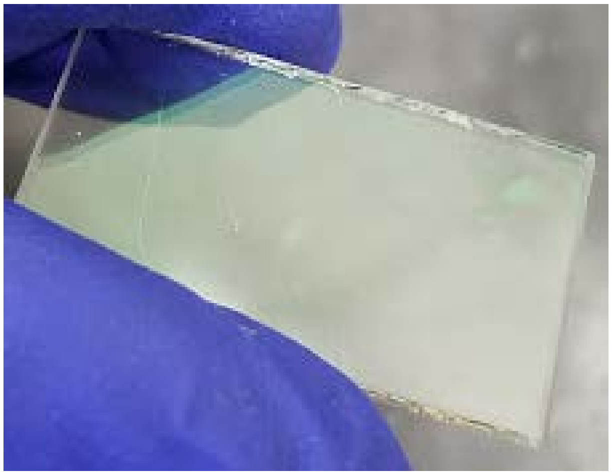

*Figure 5. ZnO coated glass sample.*

## 4.3 Methylammonium Lead Iodide Layer

Next, the $MAPbI_3$ layer was formed by a two-step process including spin coating then dip coating the spin coated sample based on the Liu, D. and Kelly, T.L., 2014 process.[30] The process used in this project consists of using two solutions. First, a spin coating solution was made, consisting of lead iodide dissolved in solution of dimethylformamide (DMF) at a ratio of 0.460 g $PbI_2$ to 1 mL of DMF. The spin coating solution is stirred and heated at 70°C for 10 minutes or until the solute is entirely dissolved to form a transparent yellow solution. Second, a dipping solution of methylammonium lead iodide in 2-propanol at a solution concentration of 0.06 mol/mL was prepared in a beaker big enough to fully dip the cell. For comparison, an alternative dipping solution was made using a powder form of MAI. A 25 mL solution of MAI/2-Propanol is created at a concentration of 10 mg/ml. With both the $PbI_2$ and the MAI solutions prepared, the processing begins by filtering with a 0.45 µm filter and then pipetting enough $PbI_2$ to cover the cell onto the ETL, about 0.2 mL. The sample is then spun coat at 3000 RPM for 15 seconds and 1000 RPM/s. The $PbI_2$ is dried for 2 minutes before being dipped into the MAI-2-propanol solution for 1 minute. During the process, the tweezers must not be submerged in the solution to avoid contamination. Compressed air at either low pressure or significant distance is then used to dry the sample uniformly. Once the processing is complete, the plain glass region is wiped clean of the absorber layer. A sample of $MAPbI_3$ can be viewed below in Figure 6. The detailed solution processing and dipping procedure can be found in Appendix A "12.3 Methylammonium Lead Iodide Layer Procedure".

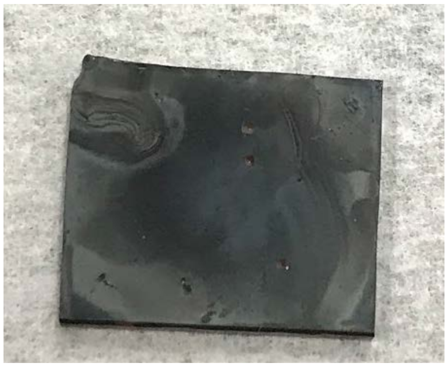

*Figure 6. MAPbI$_3$ coated glass sample.*

## 4.4 Copper Thiocyanate & P3HT

The HTL, whether it was CuSCN or P3HT, was spun coat onto the cell after the perovskite absorber layer. The CuSCN layer was based on the Jung, J.W (2015) process and methodology researched by graduate students from the WPI Nano-energy lab.[8] Similarly, the P3HT layer processing was based research conducted previously in the WPI Nano-energy lab. A spin coating solution was prepared where CuSCN was mixed in a solution of diethyl sulfide at a ratio of 40 mg/mL. The resulting mixture was placed on a magnetic stirring plate at room temperature for a period of at least eight to twelve hours or sufficient time to remove any particulates.

Spin coating was carried out with two different methods, in order to test coverage and thickness of the CuSCN layer. For both methods, a pipet was used to drop 100 to 200 µL, enough to cover the sample. Spin coating was then carried out at 500 RPM and 100 RPM/s for 60 seconds or at 5000 RPM and 1600 RPM/s for 30 seconds. The 5000 RPM method was used in comparison to the 500 RPM to examine a thin and thick layer of CuSCN. Before the CuSCN layer fully dried, the plain glass layer was wiped away with a swab. The sample was then annealed at 65°C for 10 minutes. A detailed procedure can be found in Appendix A “12.5 Copper Thiocyanate Layer Procedure”

A common HTL in solar cells P3HT, was also available in the lab. P3HT powder was mixed in with 1,2 dichlorobenzene at a concentration of 15 mg/mL, respectively. The resulting solution was stirred at 60°C until the black P3HT particles dissolved. Like CuSCN, 100-200 µL of P3HT was dropped onto the surface with a pipet to sufficiently cover the surface. The spin coater was set to 2000 RPM and 600 RPM/s for 20 seconds. After spin coating the plain glass layer was wiped away with a swab. A detailed procedure can be found in Appendix A “12.5 Poly(3-hexylthiophene-2,5-diyl)

## 4.5 Gold Evaporation

The second conductive layer, gold, was deposited with gold evaporation using standard physical vapor deposition procedures on a Varian High Vacuum Evaporator. A tungsten heater is used to vaporize gold bulk material to allow fine gold particles to coat the samples below. The evaporation was conducted at a pressure of $5.0*10^{-6}$ torr for 10 minutes. The resulting layer thickness is about 100 nm and the deposition rate is about 1.667 Å/s.

## 4.6 Solar Cell Efficiency

The PCE of the solar cells were tested by using a short-circuit voltage test followed by a voltage range test. The testing set up was a standard set up of a EC-lab Potentiostat data acquisition system connected to a Biologic SP-200 Potentiostat which is wired to the two conductive ends of the solar cell. A Newport Xenon Arc Lamp was used as the simulated sunlight source. The solar cell and lamp were spaced 13 cm apart and 14.6 cm tall to simplify calculations by making the incident power 100 $mA/cm^2$. The solar cell was affixed to a glass slide mount with the gold conductive tabs facing away from the lamp light. Two banana clip probes were connected, with the black lead on the ITO and red lead on the gold contact to complete the circuit. Example images of this setup can be seen in Figure 7.

The short-circuit voltage test consisted of turning on the entire testing system and "chopping" the light by intermittently blocking and uncovering the light to the solar cell to observe the change of voltage recorded. The spike in voltage when light is applied is the approximate short-circuit voltage. This data was used to tune the voltage range for the current over voltage range test. The voltage range test can be set from -1 V (a value less than zero) to the short-circuit voltage. The parameters of the EC-lab program was based on a past program used in the Nano-energy lab at WPI for perovskite solar cells. The program was run and a current density-voltage curve is made for the solar cell. The PCE was solved using the experimental power divided by the incident power multiplied by 100. Due to the 13 mm distance, the PCE is equal to the experimental power. The detailed procedure for PCE testing can be found in Appendix B "13.1 Power Conversion Efficiency Testing"

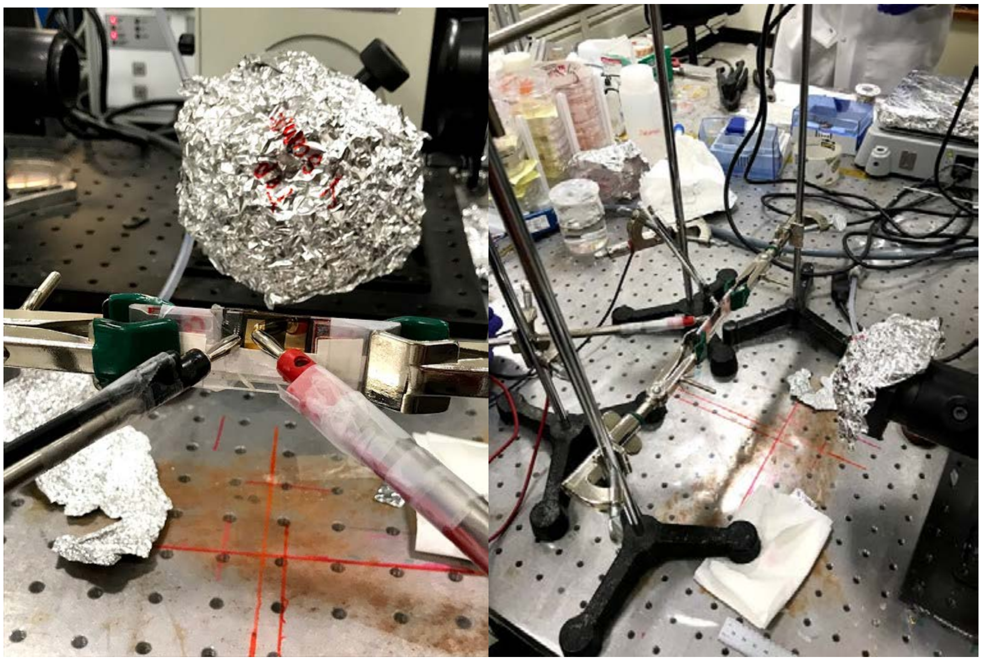

*Figure 7. (Left) Close up of solar cell sample in stand with probes attached. (Right) full PCE test set-up.*

## 4.7 Flexibility Testing

The flexibility of the cell was a fundamental part of our experiment and needed a repeatable and reliable method of comparing flexibility between samples. In our testing, we used three sample types, PET samples, Kapton samples, and staircase samples. The two methods we used for identifying failures in layers were optical microscopy and resistance measurements.

The procedure for out PET samples began by taking pre bend images in representative regions of the sample and resistance measurements of the samples. The criteria for representative regions were images of a region closer to the edge of the sample and a region closer to the center of the sample. The resistance measurements were taken using a probe attachment to the multimeter that would allow a standard force and measurement distance (1 cm) for all samples. The resistance measurement testing device can be seen below in Figure 8. In addition, these regions were centered along the perpendicular axis to the bending direction. Next, the cell was taped to the object and another piece of tape was placed to the other side of the cell to help manipulate it without making direct contact. Testing was then conducted by either bending or rolling the sample around the radii depending on the size of the radius. During rolling, it was important to wrap the cell 180° around the object to make sure the entirety of the sample was being exposed to the bend. This process can be seen below in Figure 9. The bending was conducted as a single bend around the radii (in mm); 57.8, 45.9, 31.2, 26.5, 12.4, 5.0, 3.8 and creasing the sample. The crease serves as the smallest radius of curvature possible for the given substrate. After each bend around a radius, the resistance change was tested and recorded. Once all band radii were completed, optical images were taken at 5x, 10X, 20x, 50x, and 100x in similar or the same representative regions in the pre bend imaging.

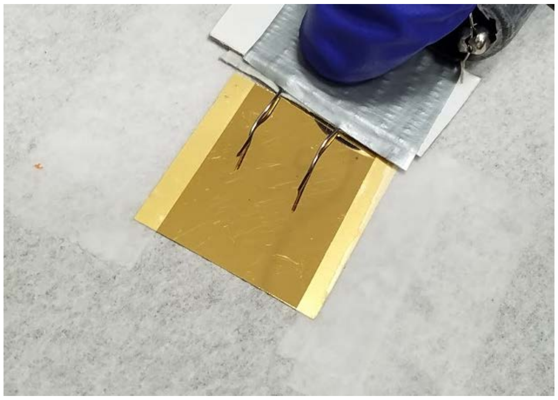

*Figure 8. Resistance testing device*

*Figure 9. Examples of sample bending.*

The second sample type tested was Kapton samples. The Kapton tape was rolled around the radii (in mm) 12.4, 10.4, 4.0, 2.6, 0.9, and creasing the sample. The same method was followed as the PET samples except no SEM images were taken. The tape was flexible enough where we needed to wrap and roll it around the radii in order to fully expose it to the bend without having it wrap around itself. This process can be seen below in Figure 10.

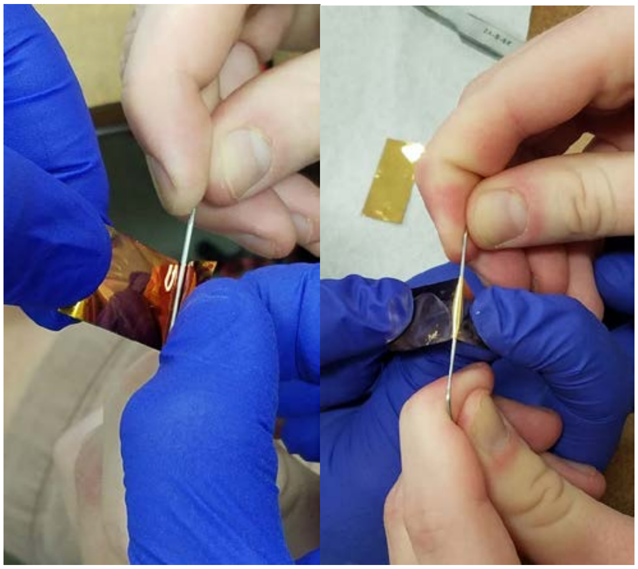

Figure 10. Example of Kapton sample bending.

The lasts tests on staircase samples utilized the same procedure as the PET and Kapton samples. The staircase cell configuration can be seen in Figure 11 below. The differences in the staircase procedure are that the resistance measurements were taken in three locations, ITO-ITO, Gold-Gold, and ITO-Gold. In addition, there were no optical images taken of the types of samples. A detailed procedure for the staircase cell flexibility testing can be found in Appendix B "13.2 Staircase Cell Flexibility Testing".

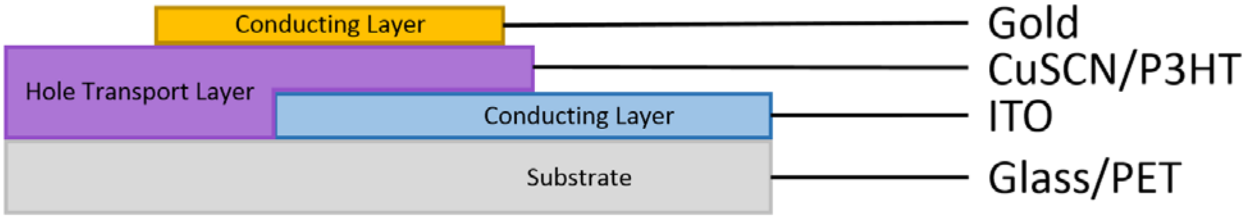

Figure 11. Diagram of staircase cell.

## 4.8 Scanning Electron Microscope Imaging

The characterization of the solar cells and single layer samples were evaluated with the use of a JSM 7000F SEM. The layer surface roughness, material structure, and layer thickness was focused on in characterization. Samples were mounted in top view orientation (layer surface perpendicular to electron beam) and in cross section view (layer surface parallel to electron beam) with double sided copper tape to affix the samples and to add a conductive layer for improved SEM imaging. The sample regions of interest in both views were equalized to the same height above the sample holder. The limiting height is determined by the thickness of the samples in the top view orientation. Below in Figure 12 are examples of the SEM samples in a sample holder. SEM images were taken in multiple regions toward the center of the sample at varying magnifications. Top view images were taken at 5,000x - 20,000x to view the material structure and the layer surface coverage. Cross section images were taken at 20,000x - 100,000x to view the layer thickness and surface roughness.

*Figure 12. Examples of SEM holder mounting with samples attached.*

# 5.0 Solar Cell Layer Processing

In order to test the efficiency of solar cells with CuSCN and test the flexibility of the cell, the solar cells needed to be repeatable. The first stage of the project required solar cell layer development to gain knowledge and skill to create each layer with consistency. The baseline knowledge and lab technique was established from literature review and personal experience from WPI and Nano-energy lab graduate students. For the overall process, our group tested all individual layers first on FTO/ITO glass and examined using SEM imaging to determine proper material structure and view layer surface features across the sample. Once the layer processing techniques worked to deposit a layer, a stepwise process of adding layer was done to address the possibility of each layer having an effect on the previous layer. After all layers were fabricated together, full solar cells were created on glass substrates. To create our final solar cell, many iterations on individual layer processing were needed to achieve parameter requirements and overcome setbacks. The work on some layers was done simultaneously from individual layer tests to actually layering the samples. This discussion overlaps in some information during the $MAPbI_3$ and CuSCN layer sections.

## 5.1 ZnO

The first layer in the set of five total layers was the Zinc Oxide (ZnO) layer. This layer was formed by a sol-gel solution processing technique to grow spherical Nanoparticles based on Liu, D. and Kelly, T.L., 2014 process.[31] The ZnO layer was the most complicated layer to create in terms of precise solution processing in the solar cell and was the most time consuming. The greatest setbacks included the learning curve to for the Nanoparticles and controlling the layer particle size.

One of the most important steps, titration duration, directly affects if the solution will precipitate ZnO Nanoparticles over the 2.5 hour temperature hold. When the solution did not have the proper 3 drops per second or the drops were not made from a lab instrument that can create round drops, the solution would not precipitate particles correctly. The resulting ZnO would be particles with little growth identifying that the particles did not surpass the initial growth threshold to develop spherical particles. In addition, the 60°C to 65°C solution temperature on a hot plate was important to assist in continue homogeneous nucleation and practice growth over the 2.5 hours. This temperature was very close to the boiling temperature of methanol which made monitoring the solution important. It was difficult to visibly identify when too much heat was added to the solution so group members needed to be proactively setting the hot plate on the lower end of the temperature range for the first 1 - 1.5 hours until the temperature stabilized as well as covering the solution with parafilm to condense methanol vapors back into solution. If the temperature was too high, the alcohol thermometer would not read a temperature higher than 65°C due to phase change of the methanol taking place. The solution would evaporate over the hold time and limit the amount of Nanoparticles formed as well as limit the overall growth of Nanoparticle size.

In terms of layer processing in the solar cell, mechanically controlling the size of the final ZnO layer became an important parameter of the layer as experiments were conducted. The first samples conducted were different coating numbers for the Zno Nanoparticles to evaluate the real processing ability of our lab and to determine the best ZnO sample in comparison to the work of Liu, D. and Kelly, T.L., 2014 process.[31] The samples conducted were of 1, 3, 5 , 10, and 15 coatings of ZnO. Images of these layers can be seen below in Figures 13-16. The samples layered well on the macroscopic scale besides visually evident large particles. The layers made in lab were in a similar thickness range as other research papers for the thin Nanometer size portion of the layer. The large particle observation was confirmed with SEM images, they were larger than 1 µm and the 5 coating layer was the best to fitting our layer parameters. The 5 coating layer had the best balance of thickness (80-100 nm for the consistent portion of the layer) to uniform surface coverage. Once successful layers were created, the next task was removing surface variation.

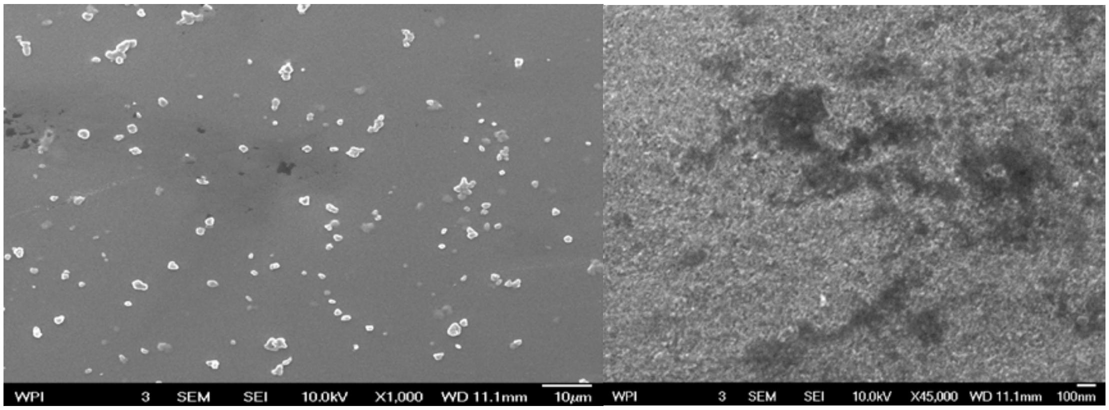

*Figure 13. 3 Coating layer of ZnO (Left) 1,000x top view of ZnO (Right) 45,000x top view of ZnO.*

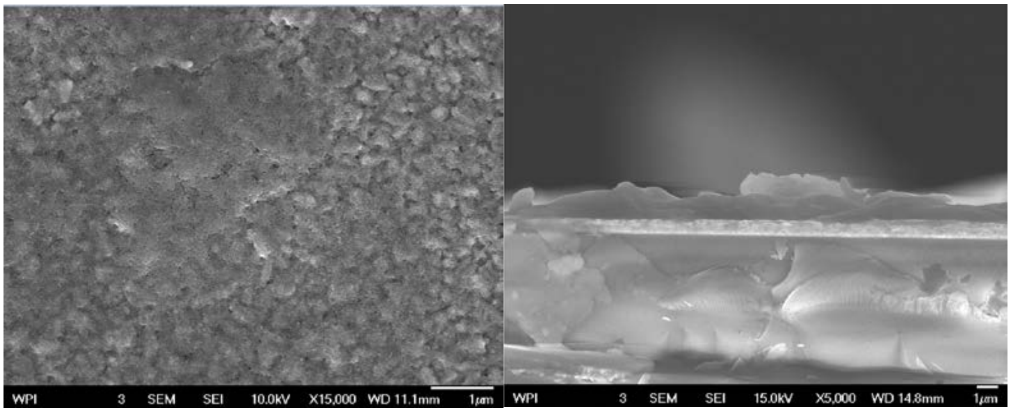

*Figure 14. 5 coating layer of ZnO with a thickness of about 80 nm (Left) 15,000x top view of ZnO (Right) 5,000x side view of ZnO.*

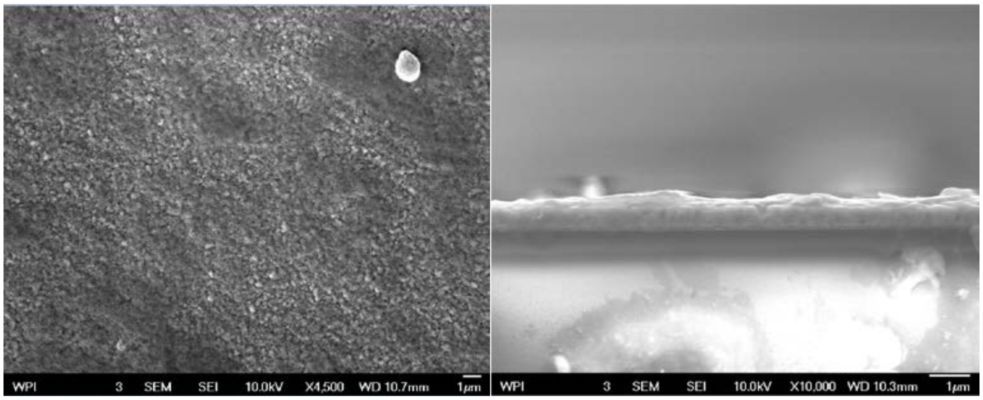

*Figure 15. 10 coating layer of ZnO with a thickness of about 120 nm (Left) 4,500x top view of ZnO (Right) 10,000x side view of ZnO.*

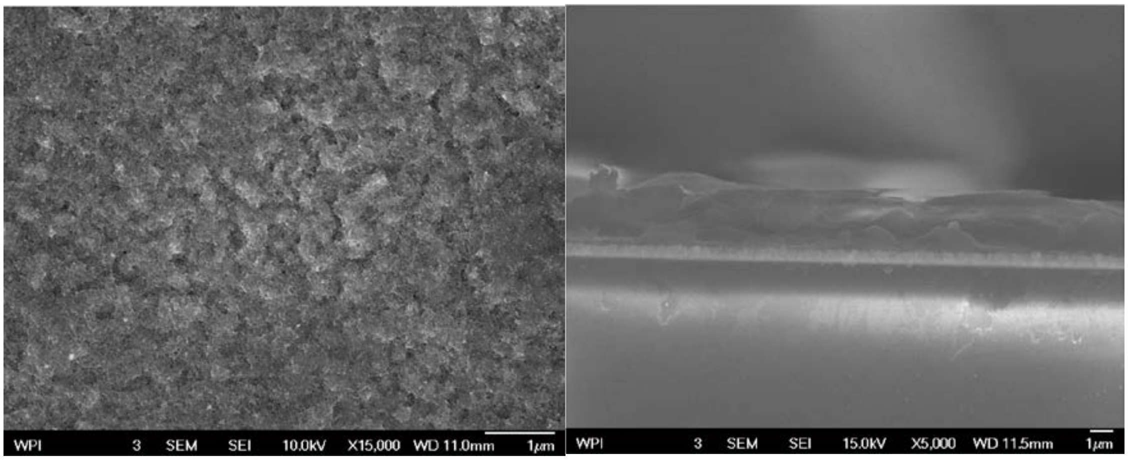

*Figure 16. 15 layer ZnO coating with a thickness of about 200 nm (Left) 15,000x top view of ZnO (Right) 5,000x side view of ZnO.*

The large particles are important to eliminate due to their ability to cause holes in future layers, the thickness variation lowers the efficiency of the solar cell, and uncontrollable surface variation would reduce consistent layer repeatability. To address this complication, three 5 layer samples were made; an unfiltered layer, a 25 µm filter layer, and a 0.45 µm filter layer. These samples were compared visually and through SEM imaging which identified the filtering had a great effect to reducing the size of particles on the layer. Examples of the effect of filtering can be compared from Figure 17 below. The 25 µm filter layer had a reduced large particle size to about 1 µm consistently and the 0.45 µm filter removed nearly all of the large particle to leave the desired 80 - 100 nm coating. With this information, a last set of samples were created using down to 0.45 µm filtering as we started processing for our $MAPbI_3$ layer. This time the layer had some particles on the final sample coating and in SEM images. We determined that the sitting period of the Nanoparticles after the 0.45 µm filter in a scintillation vial before spin coating created permanent agglomeration of the particles. Moving forward, all final 0.45 µm filtering was conducted directly before spin coating in addition to mixing of the solution to eliminate agglomeration. The filtering technique of a first 25 µm filter after

Nanoparticle solution formation and a 0.45 µm filter before spin coating allowed our group to coat ZnO layers with a good quality and consistency based on literature parameters.

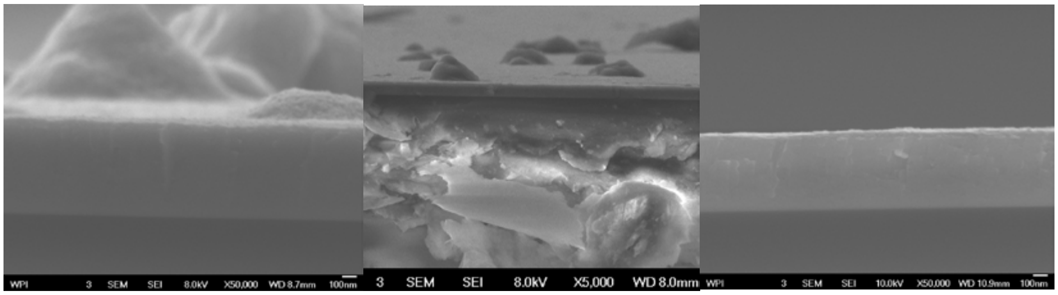

*Figure 17. (Left) SEM image of unfiltered ZnO. (Center) 25 µm filtered ZnO (Right) 0.45 µm filtered ZnO on the right.*

## 5.2 $MAPbI_3$ & $FAPbI_3$

The perovskite layer is responsible for harvesting light and therefore is essential to the operation of the solar cell. The layer structure and consistency of the layer are of utmost importance for solar cell efficiency. The major difficulties encountered in processing a working perovskite layer was preventing degradation, creating a uniform layer and producing the proper molecular structure. Our group attempted two types of absorber layers $MAPBI_3$ and $FAPBI_3$ as well as two processing types for each absorber, a spin coating layer and a two step spin/dip coating process.The first tests we performed were on $MAPbI_3$ layers via a spin coating technique based on Zhao, Y., Nardes, A.M. and Zhu, K., (2014) process and Xing, G. and Mathews, N (2013) process.[41,73] This spin coating technique yielded uniform layers but a yellow color that signified the material was not the proper structure for good transport or charges for the solar cell. Figure 18 below is an example of the first samples. The samples were determined to not have been heated enough to cause a reaction. The reaction of the materials in solution only occur once heat is added with the mixture of solvents used to make the perovskite. Before an anneal test could be done to observe the progression of structure change, there was an issue obtaining more MAI powder.

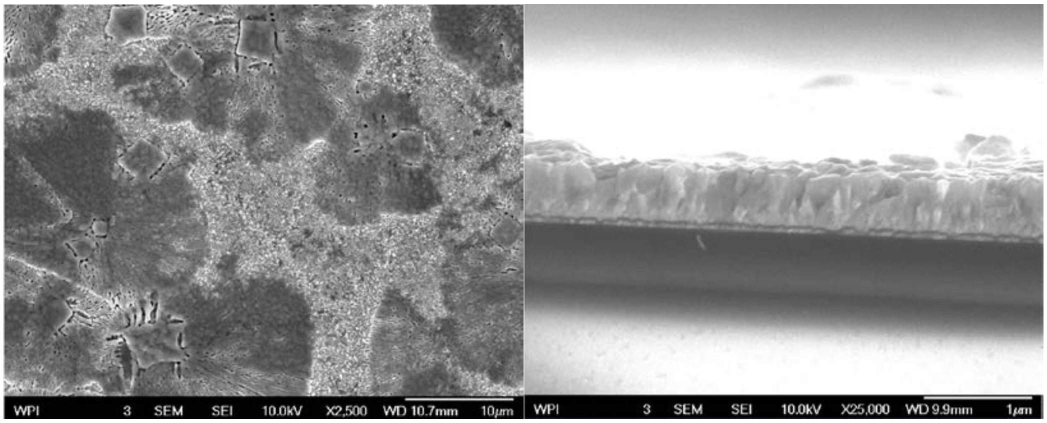

*Figure 18. SEM image of $MAPbI_3$ with incorrect Perovskite structure. (Left) Top view. (Right) Side view.*

During this intermediate phase without access to MAI we used FAI powder and $FAPbI_3$ for the absorber layer. Based on our research, $FAPbI_3$ is a similar material to $MAPbI_3$ in its PCE efficiency, band gap, and layer processing. The greatest difference between the materials is that FAI is less volatile, allowing slightly higher annealing temperatures to be used. In addition, $FAPbI_3$ is less susceptible to degradation from moisture, which made working with the material easier than $MAPbI_3$. We applied similar processing techniques and material concentrations in the solution for spin coating. The $FAPbI_3$ showed an improvement in structure during anneal temperature trials as the temperature was increased, but still not to the extent that was desired to acquire the proper structure. For the trials we conducted 100°C for 30 min, 120°C for 20 min, 150°C for 10 min , and 170°C for 5 min which had a trend of yellow to a dark orange in color. In all samples, there was some precipitates affecting the uniformity of the layer. In Figure 19 below is and image of the anneal 100°C, 120°C , and 150°C samples. One detrimental aspect to the structure improvement was that the $FAPbI_3$ had a tendency to form gamma $FAPbI_3$ (yellow color) once cooling began. This phase is the stable phase under normal conditions and the of $FAPbI_3$ is the desired structure for our solar cells. This information can be referenced in the background section “2.4.4.4 Formamidinium Lead Iodide (FAPbI3)”.

Simultaneously, a trial of heating PET was conducted to see the real max temperature threshold on the lab hot plate these substrates could handle before physical deformation occurred. Starting at 175°C the plastic visible bent from heat, this became the max temperature possible. The processing annealing threshold was determined to be less than 160°C from this point on. Due to these findings in the anneal tests and the structure transformation, we researched in literature to change our processing to a low temperature method to eliminate the use of annealing in the absorber layer.

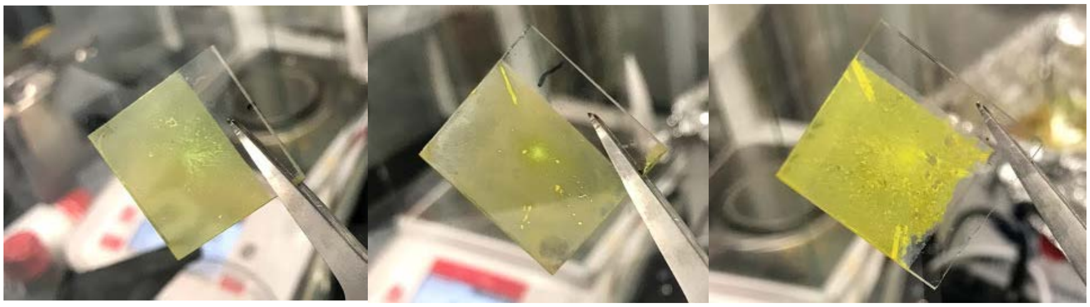

*Figure 19. Spin coated $FAPbI_3$ samples. (Left) annealed at 100℃ (Center) annealed at 120℃ (Right) annealed at 150℃.*

At this time we began experimenting with dip coating for the $FAPbI_3$ layer Liu, D. and Kelly, T.L., 2014 process.[31] We did not have the correct solvents to follow the exact literature article but we had similar chemicals to use as a substitute. The initial dip coatings were to see if this technique was worth continuing research on. Examples of these test results can be seen in Figure 20 below. The first samples showed potential as the layers became a dark brown or black color with different processing techniques but after sitting in the glovebox, the layers tended to change to a lighter color. The drawback of this process was the drying of the layer formed streaking consistently and continued the same trend of precipitates from the spin coating samples. This demonstrated that the dip coating process reactions were creating the proper material structure but something was affecting the life of the material and surface finish. We decided the solvents used were affecting the life of the layer and the correct solvents were ordered to eliminate the biggest issue of this layer. At this time, work on the CuSCN layer took over until the desired materials arrived; this work will be discussed in the next section. Once we obtained MAI again, we pursued dip coating as our chosen processing method due to the promising results achieved with the $FAPbI_3$ experiments and the negative findings in annealing found by spin coating methods.

*Figure 20. (Left) $FAPbI_3$ dip coating layer just after dipping. (Right) Same layer after sitting in the glovebox.*

The group used a liquid based MAI/2 propanol solution and the correct solvents to start the dip coating. There was success in the first set of $MAPbI_3$ , perovskite layers with the correct crystal structure but we continued to see defects in the layer. The processing was the same as the $FAPbI_3$ and with these samples we hoped to work now on surface finish. The surface defects would limit the efficiency of the solar and possibly lead to short-circuits. The second round of samples yielded yellow and orange samples after dip coating. Many different remedies were tried from changing the concentration of the dip coating solution, creating solutions right before processing so no solution reactions could happen in the glovebox, and even incorporating annealing to recover samples. Overall none of these methods worked but on inspection we noticed our concentrated MAI/2 propanol liquid solution had settled precipitates at the bottom of the container. For future solutions we made sure to stir and/or heat the MAI/2-Propanol until the precipitates dissolved back into solution. Once this was done, the layers returned to a brown color but, over time the dip solution had a chemical reaction in the glovebox and the resulting layers would slowly be a lighter color and a different structure in each sample batch on following days. We attempted to tightly seal the solution with parafilm and make the solution right before layer processing of the absorber. Examples of the container precipitation and sample change can be seen below in Figure 21 and in Figure 22.

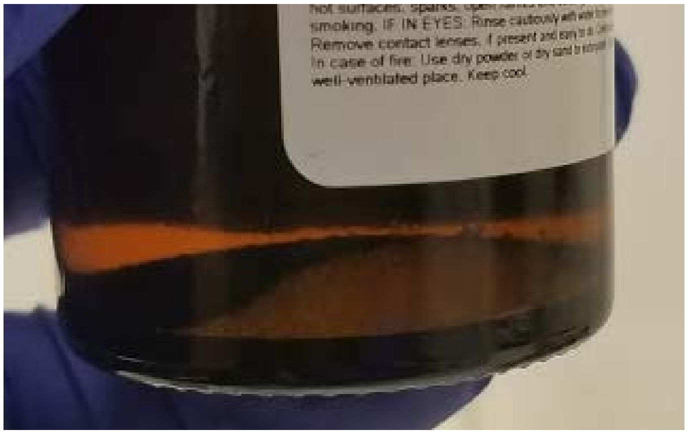

*Figure 21. The MAI/2 propanol solution with MAI precipitation resting at the bottom.*

*Figure 22. The first $MaPbI_3$ layers obtained. Sample A an old dip coating solution that initially worked. Samples B and C using a solution mixed that day. Sample D had the same parameters as B and C but was dipped in the old dip coating solution.*

At the same time the perovskite structure change occured we simultaneously had an issue with some samples exhibiting structure change to turn a white color originating from the taped side of our samples. Originally, we were taping our samples to protect the ITO portion of the cell from being covered with the other layers. The end solar cells need a clean conductive contact at each side of the solar cell to function. This structure change would only happen after dip coating so we hypothesized that the solution was having a reaction with the adhesive of the clear tape. When samples were dipped in dip solutions without tape the samples did not experience this white structure. Instead of taping we used a swab method using solvents to clean off the portion of the layer that the tape would have been. An example of the effect of tape contamination can be seen below in Figure 23. After learning about this contamination problem we made sure to prevent anything but the sample from coming in contact with the dipping solution. This would include lab tools and even more careful cleaning of supplies.

*Figure 23. Example of tape contamination after dip coating and annealing.*

After moving past the slight setbacks previously discussed, we set our focus to the precipitates in the layer. Previously, we had only been stirring our $PbI_2$ solution but with careful observations in sample trials, the precipitate appeared on the sample after spin coating, therefore disrupting layer uniformity. An example of the precipitates in the spin coating step can be seen below in Figure 24. To solve this problem, we discovered that we could heat the $PbI_2$ to 70°C continuously before each coating and filtered it at 0.45 µm. This took a couple sets of sample trials by comparing various samples by mixing the traits; heating to 70°C, not heating, stirring, filtering, and cooling before coating. The heating of the solution assisted in dissolving the solute formed from the DMF $PbI_2$ reaction, filtering removed and excess solute that could not be dissolved in solution, and heating continuously allowed the layer to be coated “hot” and cool near the end of spin coating to eliminate time for large patches of precipitate to form with localized cooling.

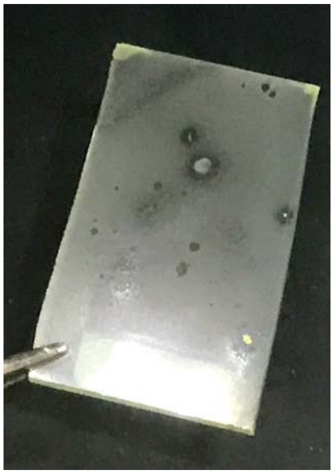

Figure 24. Example of precipitates in the $PbI_2$ spin coating step.

Some full solar cell were made from the samples with the best perovskite finishes we had so far. All of the solar cells had a solar efficiency of zero. Significant research time was used to look through all layers processing and chemicals to determine what led to nonworking cells. The most research was done on the perovskite because of a change of crystal structure in the layer with the latest sets of solar cells. It was found the DMF solvent used in the $PbI_2$ spin coating layer was affected by vapor mixing. With this identified, we moved all of our chemicals and processing out of the low ventilation glovebox and into air chemical storage and the fume hood. The samples would be subjected to an environment with water in the air but it would allow us to make working solar cell without vapor mixing occurring. In addition, we acquired a new DMF and began using MAI powder for the dip coating solution. These steps were done to eliminate the use of any materials that could have been subject to vapor mixing. From this point on all solar cell made were working cells, an example of the $MAPbI_3$ structure is below in Figure 25.

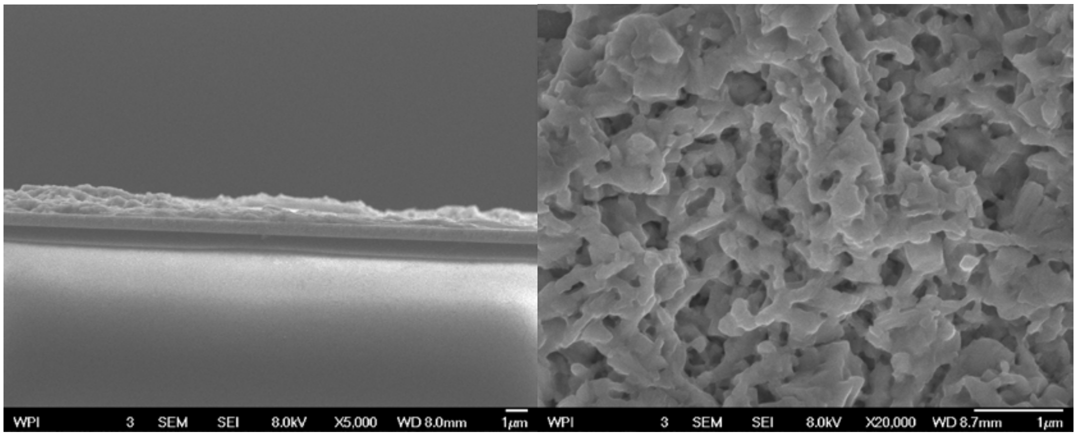

Figure 25. SEM images of the $MAPbI_3$ single layer.

The last surface finish adjustment made was focusing on drying the samples after dipping. Samples dried without air and with air tended to have areas of no perovskite or lines created from drying on the samples. To combat this we lightly dried the samples using compressed air at a tilt angle to the airflow would be towards the tweezers holding the sample. This method was adopted as a suggestion from a graduate student in the lab to use a low velocity airflow to limit lines from drying and the specific angle to limit and contamination coming from the tweezers holding the sample. This drying methodology limited the amount of drying defects created on our samples. A few of the visual cell problems we ran into are shown below in Figure 26

*Figure 26. MAPbI$_3$ layers after layer processing. (Left) Lines left in the processed layer from drying. (Right) Sample dried flat without drying lines.*

## 5.3 CuSCN

The overall intent of the project was to determine whether CuSCN is a viable material to use in a solar cell HTL. This layer needs good uniformity and thickness to adequately move holes through the layer and block elections. The important aspects of the CuSCN layer was the effect on the spin coating speed and annealing temperature of the samples. We conducted tests with a spin coating method from Yaacobi-Gross, N et al (2015) and one optimized by a graduate student in the WPI Nano-energy lab initially.[74]

First, the spin coating parameters were important to creating a good HTL layer for our solar cells. The original method from literature was spinning at a faster speed (CuSCN 800 RPM) and for a shorter period shown below in Figure 27. These samples did not have the best surface coverage and high surface roughness so we attempted making layers with a slower spin speed and longer spin time. This slower process (CuSCN 500 RPM) developed in the Nano-energy lab had a thicker layer and a lower surface variation shown in Figure 28. In trials with the CuSCN in other solar cells, it was found that the slower speed process also had a better efficiency. For most of the project we used this 500 RPM spin speed as the base processing method.

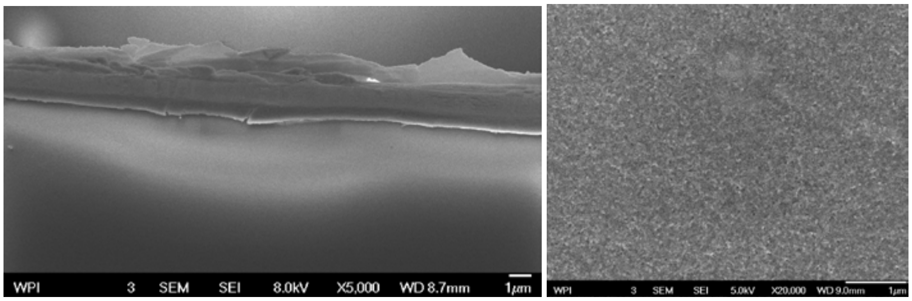

*Figure 27. SEM images of the CuSCN 800 RPM sample. (Left) Side view. (Right) Top view.*

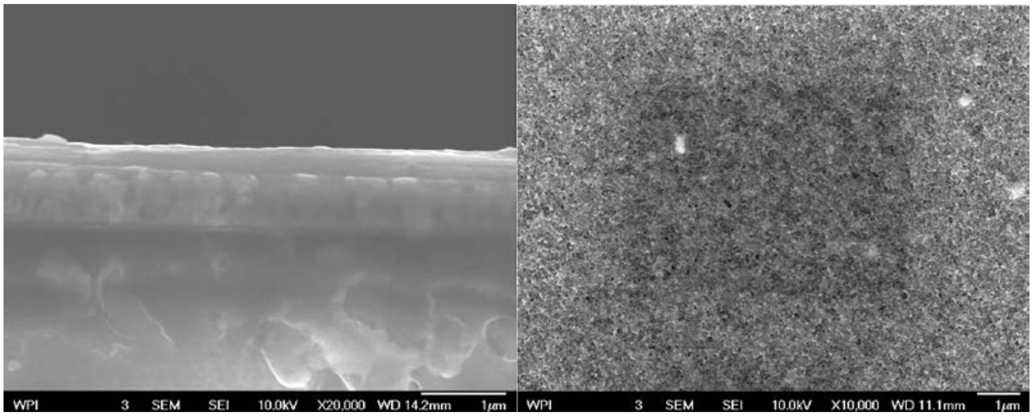

*Figure 28. SEM images of the CuSCN 500 RPM sample. (Left) Side view. (Right) Top view.*

The second area of interest for the CuSCN became the annealing temperature for the layer because of the issues heating the perovskite discussed earlier. Many sources in literature called for a 100 - 120°C anneal, but it was found through an annealing temperature trial of heating the $MAPbI_3$ layer to have a limit of less than 100 °C. Samples were heated at 90°C, 100°C, 110°C, and 120°C with and without CuSCN. The results with and without CuSCN were the same, at 90°C the sample retained a brown color while the temperatures at 100°C and greater exhibited color changes to orange and even yellow. Due to these findings, more literature review was conducted and CuSCN techniques without annealing were found. A faster spin coating method (CuSCN 5000 RPM) from Jung, J.W (2015) was proportionally similar to the 500 RPM method we were using.[8] We ran single layer trials of CuSCN at a 5000 RPM speed for a short duration with annealing at 65°C for 10 min and no annealing. As a comparison the 500 CuSCN was annealed at 100°C and at 65°C for 10 min each. From these trials, all CuSCN layers annealed at 65°C for 10 min visually dried and had the desired structure. The 65°C anneal is not high enough to cause and degradation or structure change in the $MAPbI_3$ layer. Moving forward, both the spin speed CuSCN coatings were used moving forward for a thick and thin layer comparison with annealing at 65°C. Overall, the CuSCN layer is difficult to distinguish features on due to its very transparent nature. In Figure 29, a sample can be seen on glass. Most samples were made on the $MAPbI_3$ layer to identify changes in the CuSCN layer easily.

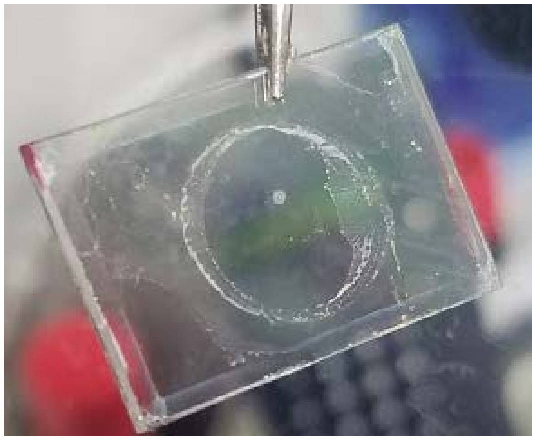

*Figure 29. CuSCN on ITO glass only visible due to inconsistencies in layer thickness and residue from the CuSCN.*

## 5.4 P3HT

The P3HT was used as a comparison HTL that is commonly used in flexible solar cells and the layer has a solidified processing technique used in the Nano-energy lab. There was no additional research in processing for this layer; the method used in the lab deposited a consistent layer with little surface variation. This processing method was utilized in all trials. The method created layers with good efficiency for HTL comparison in our project.

## 5.5 Complete Solar Cells

Once the all layers were individually evaluated full layer solar cells were created. The parameters of most interest to the solar cell layers are the end structure of each layer and layer thickness. If the structure is not correct or the thickness is outside of the performance range, the solar cell efficiency and mechanical properties will suffer. A summary table of the thickness goals for our project can be found below in Table 8.

*Table 8. Layer thickness parameters*

| **Solar Cell layer** | **Thickness Range (nm)** | **Optimal thickness (nm)** |
|---|---|---|
| ITO (on glass) | N/A | 60 |
| ZnO | 20 - 70 | 25 |
| $MAPbI_3$ | 200 - 400 | 300 |
| CuSCN | 20 - 50 | 40 |
| Gold | 80 - 120 | 80 |

Figures 30 and 31 below show images of complete cells with a P3HT HTL and a CuSCN 5000 HTL. These images are a side-by-side comparison of the two different HTL's observed in our research. Both cells went through the same processing for each layer except the HTL. The absorber is by far the thickest layer in both solar cells, being around 250 nm thick, with the underlying ZnO layer just under half that thickness between 90-120 nm. Despite the two different materials, the HTL thickness in both cells have remarkably similar values. Both CuSCN 5000 and P3HT were coated on the cell at about 60 nm thickness. Throughout our samples the gold was very consistent around 80nm thick as shown in the CuSCN 5000 cell; because of the gold overhang the thickness was measured to be around 120 nm in the P3HT cell.

*Figure 30. Three working P3HT solar samples.*

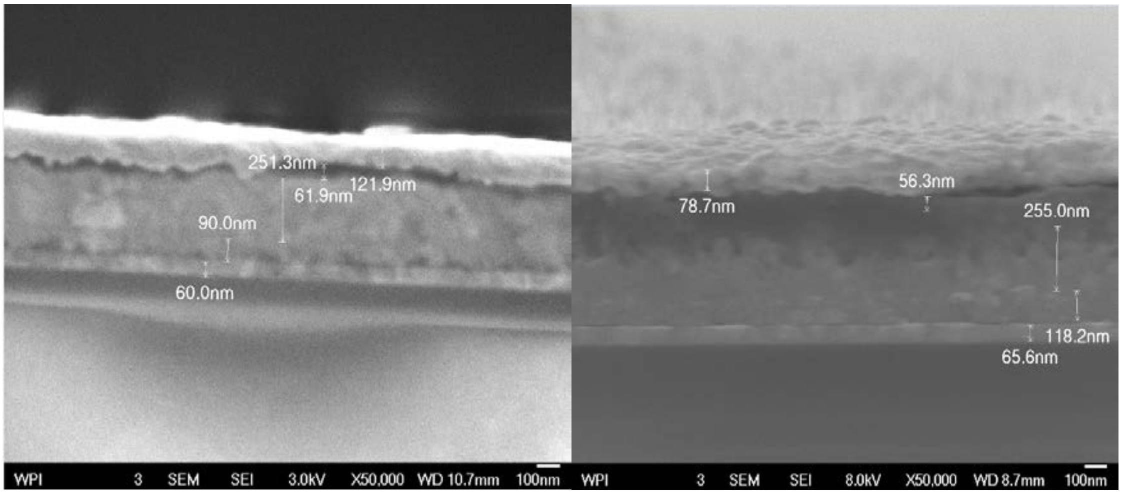

*Figure 31. SEM Images of complete solar cells. (Left) P3HT sample 28A as above. (Right) CuSCN 5000.*

In the solar cell the two conductors were fixed values due to the ITO being pre coated and the gold evaporation being applied for a specific duration. SEM imaging showed the ITO thickness to be approximately 60 nm. Similarly, the final gold layer was also limited in control of the layer's thickness. The gold evaporator was run by graduate students in the Nano-energy lab at WPI resulting in a gold layer of approximately 80 nm. Measuring the layer thickness of gold proved difficult in SEM imaging as sometimes the sample would have gold overhang from the break when it was cut making it impossible to accurately measure.

The portion of the solar cell we had control of was the ZnO, $MAPbI_3$, and CuSCN layers. Each layer needed to be at the optimal thickness or in the thickness range and have consistent structure to maximize the cell’s potential efficiency. Besides performance, the importance of layer thickness is to limit the possibility for short-circuiting between layers. For example, electron and hole transport layers, ZnO and CuSCN, that were too thick would limit the cell’s ability to send charges to the conductors and create a working current. Our solar cell was in the range of optimal performance for the $MAPbI_3$ layer but the CuSCN and ZnO layers were outside of the range. The higher thicknesses were not large enough to effect mechanical properties or cause short-circuiting but it did limit solar cell performance. Another important observation made is our absorber layer did not have a full reaction for the absorber layer causing a two material layer. The separation is most likely half $MAPbI_3$ and half $PbI_2$. Our group did not perform X ray diffraction to determine each material, but it is possible that our dip coating solution only penetrated half of the $PbI_2$ thickness in processing. Even with some layers outside of the optimal performance range the solar cells had a solar efficiency and these findings will be discussed in the next section.

# 6.0 Testing Results

In our project, we conducted two tests to evaluate CuSCN as a HTL in flexible perovskite solar cells in comparison to a common HTL, P3HT. We focused on PCE testing to create a working solar cell and flexibility testing to see the extent of flexible applications CuSCN solar cell could be used for.

## 6.1 Power Conversion Efficiency Testing

The PCE testing was our method of measuring the sample for its actual functionality as a solar cell. The highest PCE we were able to obtain was an efficiency of 0.26% using P3HT and 0.001% using CuSCN. Images of these solar cells can be referenced above in section "5.5 Complete Solar Cells" Figures 30 and 31. Both cells encountered complications in material contamination, layer thickness, and even incomplete reaction of the absorbing substrate. Our results and testing using the "chop testing" method showed us that some of our cells were reactive to light but not to the extent that we initially hoped. Figure 32 shows the I-V curve and PCE data of our best P3HT cell. The dip in these graphs represent the chop testing described in the methods section where it was confirmed that our setup was reacting to the light source. A table of the raw data for our 6 solar cells can be referenced in 12.1 Appendix C "Table 10 Power Conversion Efficiency Data".

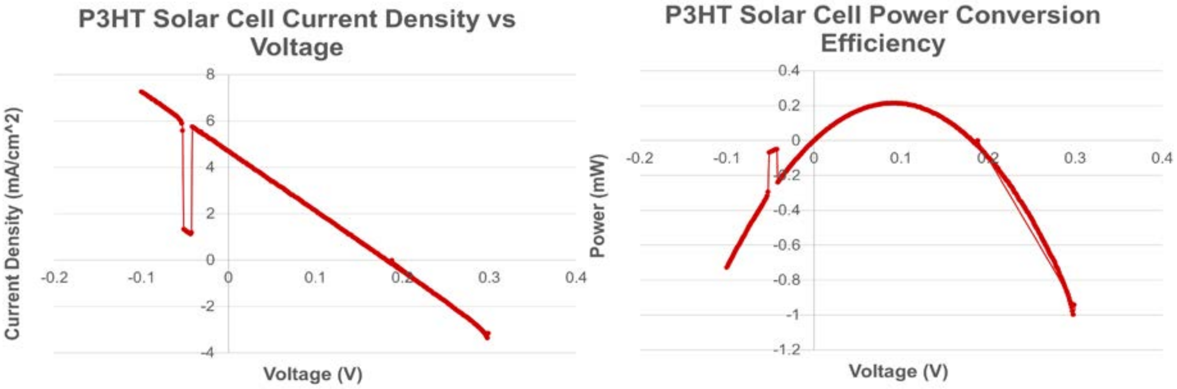

*Figure 32. (Left) Best cell current density. (Right) Best cell power conversion efficiency.*

During the dip coating process for the absorber, we noticed that SEM images showed a divide within what should be a single layer as well as a thinner absorber layer and a larger HTL than we initially hoped to create. We attribute the divide to the possibility that the MAI did not react fully with the $PbI_2$, resulting in a half absorber layer which could have impeded the ability for current to flow. This divide can be seen in the CuSCN solar cell absorber layer in Figure 30 above. In addition, the thinner and the solar cell and slightly thicker transport layers would reduce the amount of charges moved to the conducting bands. The solar cells were also fabricated in open-air lab environment, which added moisture degradation a problem. We learned through our research that $MAPbI_3$ is reactive to both light and moisture content, and expected it to reduce the values we could achieve during testing.

## 6.2 Flexibility Testing

Flexibility testing was conducted to evaluate if CuSCN could be used in flexible solar cells and how this flexibility compared to P3HT. In our project three methods of flexibility testing were used, these are classified as PET samples, Kapton samples, and staircase samples.

First, before we tested the samples, an ITO PET sample was bent through the same radii as the PET samples. The data showed the layers would crack perpendicular to the direction of bending across the entire sample at the lowest bend radii or at the crease radius of curvature. In most solar cells, the ITO layer is the most brittle and limits the flexibility of the solar cell. Once the conductors break, charges cannot be transported horizontally across the layer to the circuit. In our PET and Kapton samples, layers of the conductors individually and the three HTL's of interest with gold deposited on top were tested for resistance across the gold contact. The Kapton samples were not tested for ITO resistance changes because we could not deposit this layer on a different substrate. In both types of samples, cracking was not seen in an optical microscope in the gold layer until the samples were creased. This demonstrated that the gold layers ability to resist striations and cracking was not assisted by either HTL layer. To qualify this fact, images were taken of the top view so cracks in the vertical direction would be difficult to see and with an optical microscope we are unable to see Nanoscale cracking. The only cracking seen would be micro scale and larger that would be detrimental to a solar cell's ability to function. This is the reason resistance measurements were used as an indirect measurement method across the surface for defects that could affect charge transport.

The resistance measurements were standardized with the testing device described in the methods chapter. This measured the resistance with the same force and at the same distance for all samples. The consistency of resistance measurements means that there was no real mechanical failure within the cell to affect charge transport. Only when completely creasing and scratching the gold layer did we see increases in resistance. We attribute this to the durability of the gold layer and the inability of resistance measurements to identify minor cracking within the cell. Overall, these two tests did not give us conclusive results for the role HTL plays in assisting or limiting mechanical flexibility.

The last testing method was the staircase sample type. This sample was able to give us insight into the interface between the HTL and conductive layers. The design of the staircase cell was inspired by our curiosity about defects in layers and layer separation during bending. Previously, we had identified layer separation as an important result of flexibility testing but had focused more on layer cracking. Along with this, the staircase is very similar to our full cells configuration except it excludes the ETL and absorber layer. To focus directly on layer separation we designed this cell so that we could easily measure layer resistance with less error. The three resistance measurements we took were for the Gold to Gold, ITO to ITO, and Gold to ITO. The first two types of measurements were a baseline measurement to see if there was any cracking occurring. The Gold to ITO measurement allowed us to see if the HTL was undergoing any separation or and layer defects during bending because it mimics the path of a charge in working solar cell. The resistance moves horizontally through each probe contact on the conductive layer until the region of least resistance is found, then the circuit connection happens in vertical travel from the ITO to HTL to gold layers.

Using our data from the staircase testing, we created graphs to illustrate the effect of decreasing bend radius on resistance. There are three bars for each radius to show the different resistance measurements done. Two different scales for resistance were created to allow all the data to be seen. The graphs below in Figure 33, 34, 35 are for the P3HT, CuSCN 500RPM and CuSCN 5000 RPM. The full data values for all three tests can be referenced in 12.1 Appendix C Tables 11 - 13.

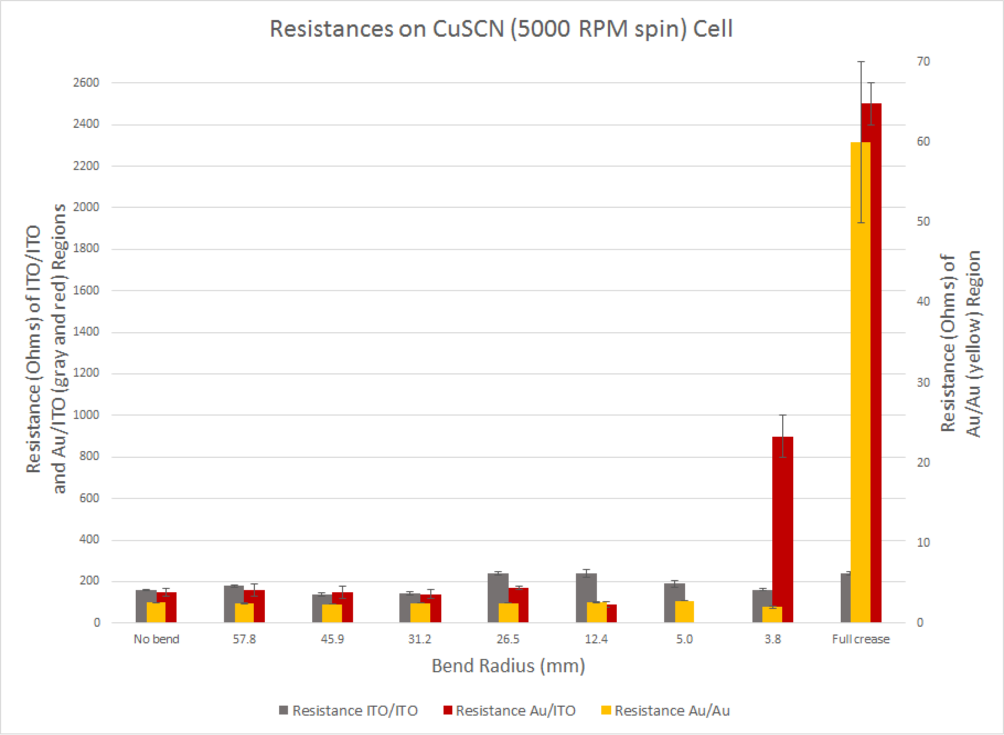

*Figure 33. Resistances on CuSCN (5000 RPM spin) cell.*

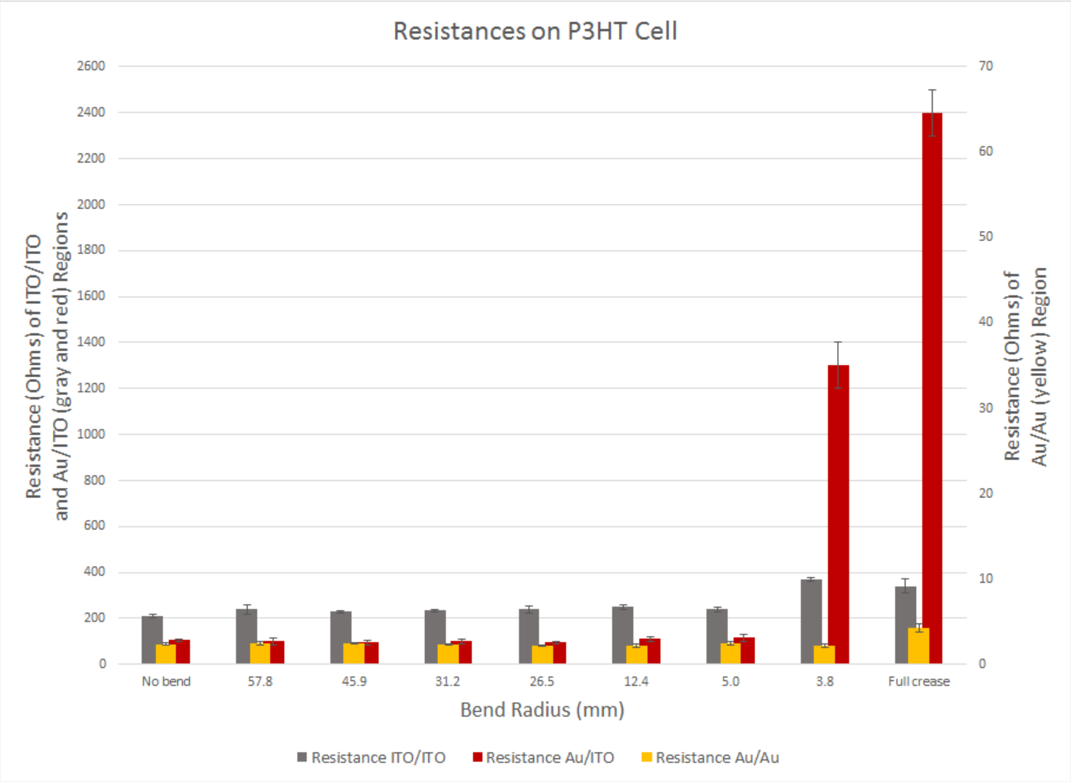

*Figure 34. Resistances on P3HT cell.*

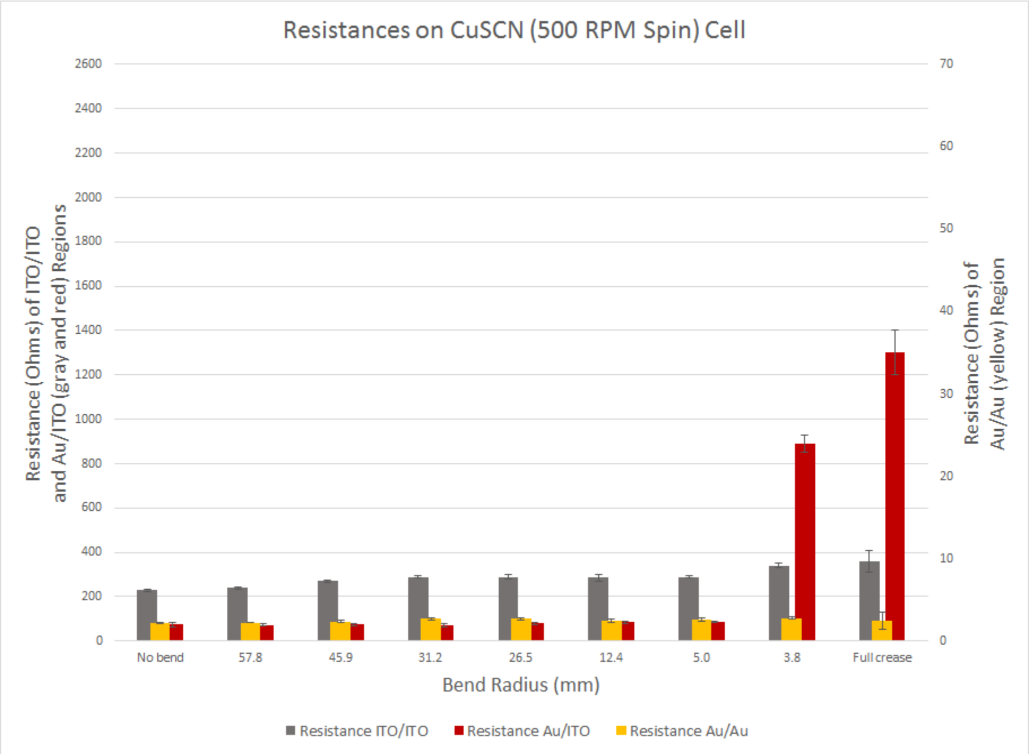

*Figure 35. Resistances on CuSCN (500 RPM spin) cell.*

The graphs identify that the ITO and gold results held at similar value at all bent radii except the gold on the 5000 CuSCN cell. This data is consistent with our findings in the first two sample types discussed previously. In comparison to the other two tests, the change in the Gold to Gold measurement looks to be an outlier. More testing would need to be conducted to check this data point. The most important data trend to observe is the spike in resistance from Gold to ITO occurs at the smallest bend radius and the full crease. This allows us to conclude that the spike in resistance between the Gold and ITO is from some sort of layer separation between the HTL and the conductive layers or a major layer defect in the HTL layer itself. During our project, we did not have the opportunity to examine the samples in a SEM to view the exact mechanism of failure in the layer or between layers. Our conclusion is only based on the resistance change of the staircase cell and the findings of the resistance change for the conductors themselves from the previous PET and Kapton samples. All three of the samples tested showed extremely similar trends with regards to when the resistance spiked and the magnitude of the resistances. It can also be concluded that the HTL is the limiting factor in this cell and that layer separation is most likely a greater concern than cracking in the HTL layer. Although this is inconclusive in terms of which HTL is more flexible, it does show that CuSCN's flexibility is comparable to P3HT. In addition, P3HT is used in many flexible perovskite cells and has been proven in literature to work well under bending. The similar data between the two HTL's is a sign that CuSCN could be a good HTL for flexible solar cells in terms of mechanical durability in bending.

# 7.0 Project Complications

A glovebox was used in our project to limit water degradation to the perovskite layer in our solar cell and eliminate toxic lead vapor from entering the lab environment. Using the glovebox throughout the project was cumbersome, as it needed to be purged of all moisture before proceeding with solution processing and spin coating of the $MAPbI_3$ layer. This was measured with a humidity sensor placed in the glovebox. While accurate, this sensor read oxygen percentage of the glovebox's atmosphere, the notion being that no $O_2$ molecules signifies no $H_2O$ molecules present in the glovebox. The sensor did not read moisture content directly, so it could not account for moisture of any other chemicals that were stored in the glovebox.

The glovebox also lacked adequate ventilation to cycle out the interior atmosphere. In order to reduce moisture content, pure nitrogen gas was forced into the box from a compressed tank. The lab's vacuum system would then be activated to draw out the entirety of the glovebox's atmosphere. This would ideally ensure that the interior atmosphere would be nearly 100% nitrogen gas. Besides the door to pass through chemicals and materials, no other openings were present on the glovebox to allow for more ventilation. Leftover vapors could cause contamination with the chemical bottles in the box. It was also later discovered that the spin coater tended to retain vapors within its casing that were leftover from previous spin coating processes. These vapors were not affected by the moisture removal process and would later affect subsequent spin coating processes until the casing was cleaned out, though how or exactly what vapors were present remains unknown.

While it was difficult to remove the unwanted vapors from the glovebox, it was also difficult to keep the glovebox at low moisture content and near-pure nitrogen atmosphere. Leaks in the glovebox's structure typically prevented moisture content levels below certain percentages, rendering the fabricated absorber layers useless or low quality. The glovebox leaks consisted of on the left side at a door, in tears in the gloves, and along the back panel of the glovebox. In Figure 36 examples of glovebox leaks can been seen.

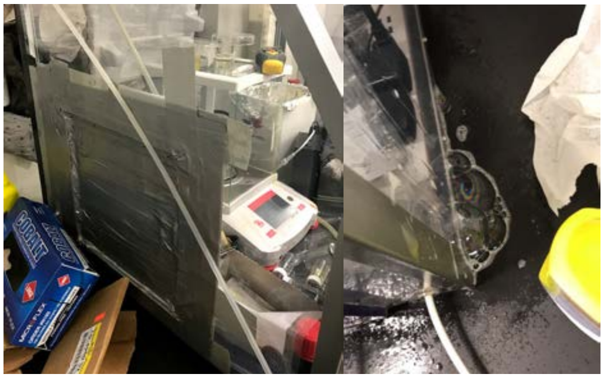

*Figure 36. (Left) Leaking door on glovebox. (Right) Bubbles from soap water test for gas leaking on the bottom of the glovebox.*

More ‘bad chemicals’ were later discovered that were related to the glovebox issues in terms of limited ventilation. For instance, the first iterations of the process for the absorber used DMSO to make a solution that combined the MAI and $PbI_2$ in a single step before spin coating. However, poor early results from SEM imaging suggested issues with the process or the chemicals. Molecular sieves were added to DMSO beforehand to absorb any minute $H_2O$ molecules that might have contaminated the DMSO and thus the $MAPbI_3$. Later in the project, DMF replaced DMSO as a solvent and was found to not create the correct chemical reaction with lead iodide. The most likely reason for this was the low ventilation in the glovebox causing vapor mixing with the DMF solvent. Once a different DMF solution was substituted in, the resulting absorber layer had superior consistency and color compared to previous results.

Research and background knowledge suggested that the created cells would be very fragile and susceptible to degradation. In addition to the multitude of glovebox precautions, there were extra steps to be taken when handling samples outside of the glovebox. It was a known precaution to take that the combination of moisture and air would accelerate the decay rate of the cell. In order to deal with both aspects, the samples were placed in a plastic petri dish and then aluminum foil was wrapped around the dish, blocking all light. The wrapped dishes were then placed in vacuum sealable bags to remove air and moisture. This allowed the cells to survive long enough to have them PCE tested. However, even PCE testing was carried out too slowly to avoid degradation. PCE and resistance results declined as more tests were carried out on each sample.

After the complications found using the glovebox to create the cells, it was decided to try the exact same processes inside a fume hood to re-evaluate the usefulness of the glovebox. The fume hood would prevent lead contact but would not necessarily isolate the samples from moisture. At this point, the $MAPbI_3$ processing had been performed a sufficient amount of times to be optimized and reduce the odds of moisture contamination. Multiple successful samples produced in the fume hood led to the decision to abandon the glovebox for the remainder of this project.

# 8.0 Conclusion and Recommendations

At the beginning of our project, we focused on layer by layer testing to change our procedures and perfect them. Most of our project was trial and error for each step of the process, sometimes extensively so in the case of our absorber layer, which we changed weekly, and even in our final cells was still imperfect. Even procedures that we found outlined in our research before were modified to better fit our lab environment and the tools we had available. Here we outline our conclusions and further recommendations for the creation of these perovskite cells as well as insight into why we think we ran into some of the errors we had.

The PCE testing we conducted near the conclusion of our project showed that both P3HT and CuSCN worked as solar cells with the layer structure that we developed earlier in the project. The final results of CuSCN reaching only 0.001% and the P3HT at 0.26% was much lower than we expected especially when compared to the 10% efficient CuSCN cells we discovered in literature. We made multiple cells of CuSCN and P3HT and due to the trends in efficiencies between the two we were able to conclude that P3HT was reliably more efficient than CuSCN using the procedures that are in Appendix A. There was no remarkable efficiency difference between the thin and thick CuSCN layers. In the future, there is still much that could be done with improving layer consistency for the CuSCN besides just modifying the spin coating procedure as we did. After conducting the PCE testing we took SEM images of our final samples and saw that the methylammonium lead iodide perovskite layer had characteristics that showed it was either degraded or otherwise not the same layer throughout.

The methylammonium layer exhibited a dark and light half in the SEM image, which identified a disparity between the structure of the layer's top and bottom. If the layer is optimized to have the correct methylammonium lead iodide structure the solar cell efficiency will increase drastically by our predictions. Because of our two step spinning and then dipping procedure outlined in appendix A we think the $PbI_2$ layer did not fully react with the MAI, leaving unreacted $PbI_2$ on the cell which would cause an interruption in the energy generation. By creating a thinner $PbI_2$ layer during spin coating this could result in a more complete reaction when the sample is dipped. Figure 37 shows the SEM image of the layer divide.

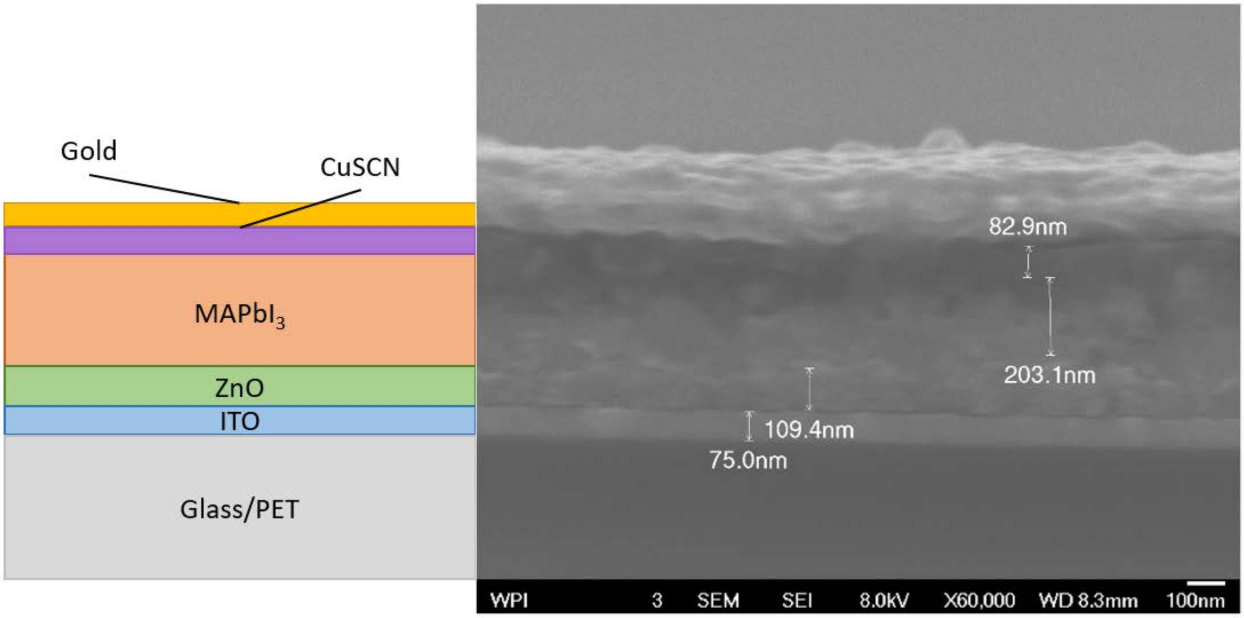

*Figure 37. SEM image of CuSCN showing layer inconsistency in the* $MAPbI_3$ *layer.*

The environment the solar cell layers were fabricated in was crucial to our project. Because of the degradation of the $MAPbI_3$ layer, we initially started working with that layer in a large glovebox that had a vacuum out and a line in that fed either Nitrogen or Argon. The glovebox was monitored using an oxygen sensor and was pumped full of either of the inert gases; however, the oxygen monitor did not monitor the humidity or any other chemicals in the system which proved to have significant drawbacks. All the work we conducted in the glovebox turned out contaminated or otherwise troublesome due to the clumsiness of having to operate in the box. As the glovebox was operated, it was the most significantly detrimental part of our project and without improvements is more likely to inhibit than improve further tests of this nature.

A glovebox with an automated ventilation system would be the ideal scenario to limit water contamination in the solutions and solar cell layers as well as removing chemical vapors. An alternative is using a fume hood to allow chemical vapors and water vapor to be ventilated away from chemicals and samples. As in our project, we used the fume hood in the lab and had our first successful cells but with the acknowledgement that they would likely degrade faster than any successfully made in a truly inert setting.

During the flexibility testing, cells were examined via optical microscopy and measurement of resistance changes. The optical imaging proved to be fruitless in being able to show visual difference in structure of the cells before and after bending. Our conclusion therefore relies more heavily on the changes in resistance we could observe and showed us how the HTL material affects the durability of the cell. Through the resistance testing, we were able to examine layer separation between the HTL and the conductive layers of the cell. The CuSCN performed very similarly to the P3HT, which showed that despite the differences in PCE testing the two layers were interchangeable mechanically. This similar flexibility in both HTLs and the fact that P3HT is HTL used in flexible solar cells gives CuSCN potential as a cheaper alternative to common expensive HTL materials for thin film solar cells.

The resistance testing for our flexibility testing was an indirect test so we recommend having bend tests with SEM images to see the actual cracks or layer separation and bending, in parallel testing PCE would yield direct results of the effect of bending. The SEM images will return much more information at the Nano and micro level than we were able to achieve on the optical microscope. These two methods would add significant data on perovskite solar cells with a CuSCN HTL layer in terms of bending and its effect on material structure. The techniques would yield visual qualitative data on the effect of bending to see actual mechanisms that happen in and between the layers as well as a macroscopic performance changing if the current density changes as a function of voltage for the bending solar cell. Incorporating these recommendations into future work will assist in a complete conclusion on how copper thiocyanate effects a flexible perovskite solar cell.

# 9.0 References

1. Tavakoli MM, Tsui K, Zhang Q, et al. Highly efficient flexible perovskite solar cells with antireflection and self-cleaning Nanostructures. *ACS Nano*. 2015;9(10):10287-10295.
2. Susrutha B, Giribabu L, Singh SP. Recent advances in flexible perovskite solar cells. *Chemical communications (Cambridge, England)*. 2015;51(79):14696-1477.
3. Estimated U.S. energy consumption in 2016. *Lawrence Livermore National Laboratory*. 2017.
4. Solar industry research data. SEIA Web site. /solar-industry-research-data.
5. Rühle S. Tabulated values of the Shockley–Queisser limit for single junction solar cells. *Solar Energy*. 2016;130:139-147.
6. Green MA. Recent developments in photovoltaics. *Solar Energy*. 2004;76(1):3-8.
7. Vos AD. Detailed balance limit of the efficiency of tandem solar cells. *J Phys D: Appl Phys*. 1980;13(5):839-846.
8. Jung JW, Chueh C, Jen AK-. High-performance semitransparent perovskite solar cells with 10% power conversion efficiency and 25% average visible transmittance based on transparent CuSCN as the hole-transporting material. *Adv Energy Mater*. 2015;5(17).
9. Optical transmittance - definition and formula. AZO Optics Web site.
10. Smith JG, Connell HW, Watson KA, Danehy PM. Optical and thermo-optical properties of polyimide-single-walled carbon Nanotube films: Experimental results and empirical equations. . 2005.
11. Polyester plastic. Prospector Web site. https://plastics.ulprospector.com/generics/37/polyester.
12. ITO-coated PET film. Thorlabs Web site. https://www.thorlabs.com/newgrouppage9.cfm?objectgroup_id=9535.
13. Faraj MG, Ibrahim K, Ali M. PET as a plastic substrate for the flexible optoelectronic applications. *J.Optoelectron.Adv.Mater*. 2011;5:879-882.
14. Polyesters. Polymer Properties Database Web site. http://polymerdatabase.com/polymer%20classes/Polyester%20type.html. Updated 2015.
15. GoodFellow polyethylene naphthalate (PEN) film. Matweb Web site. http://www.matweb.com/search/datasheet.aspx?matguid=60dc5dfcf5ba48f9bb4fe2fc7d7dd4bf. Updated 2017.
16. Kapton. Dupont Web site. http://www.dupont.com/content/dam/dupont/products-and-services/membranes-and-films/polyimde-films/documents/DEC-Kapton-summary-of-properties.pdf. Updated 2017.
17. Lozano A, de Abajo J, de la Campa J, Guillén C, Herrero J, Gutiérrez M. Thin-film polyimide/indium tin oxide composites for photovoltaic applications. *Journal of Applied Polymer Science*. 2007;103:3491-3497
18. Ensinger TECASINT 4011 polyimide, yellow (PI). MatWeb Web site. http://www.matweb.com/search/datasheet.aspx?matguid=f309af36d0cc402abec12098834a4cab.
19. Guo W, Xu Z, Zhang F, Xie S, Xu H, Liu XY. Recent development of transparent conducting Oxide-Free flexible Thin-Film solar cells. *Advanced Functional Materials*. 2016;26(48):8855-8884.
20. Poorkazem K, Liu D, Kelly TL. Fatigue resistance of a flexible, efficient, and metal oxide-free perovskite solar cellElectronic supplementary information (ESI) available: Materials, device fabrication and characterization procedures, absorption spectra, pXRD patterns, J-V curves, results of fatigue resistance and bending radius tests, SEM images, organic solar cell performance data, statistical test results, data for devices on ITO electrodes.
21. Yang Y, Han C, Jiang B, et al. Graphene-based materials with tailored Nanostructures for energy conversion and storage. *Materials Science and Engineering: R: Reports*. 2016;102(Supplement C):1-72.
22. Seo H, Kim H, Lee J, et al. Efficient flexible organic/inorganic hybrid perovskite light-emitting diodes based on graphene anode. *Adv Mater*. 2017;29(12):n/a.
23. Hu L, Hecht DS, Grüner G. Carbon Nanotube thin films: Fabrication, properties, and applications. *Chem Rev*. 2010;110(10):5790-5844.
24. Ahn J, Hwang H, Jeong S, Moon J. Metal-Nanowire-electrode-based perovskite solar cells: Challenging issues and new opportunities. *Adv Energy Mater*. 2017;7(15):n/a.
25. Guo F, Azimi H, Hou Y, et al. High-performance semitransparent perovskite solar cells with solution-processed silver Nanowires as top electrodes. *Nanoscale*. 2015;7(5):1642-1649.
26. Hu L, Kim HS, Lee J, Peumans P, Cui Y. Scalable coating and properties of transparent, flexible, silver Nanowire electrodes. *ACS Nano*. 2010;4(5):2955-2963.
27. Guo F, Zhu X, Forberich K, et al. ITO-free and fully solution-processed semitransparent organic solar cells with high fill factors. *Adv Energy Mater*. 2013;3(8):1062-1067.

28. Kim A, Lee H, Kwon H, et al. Fully solution-processed transparent electrodes based on silver Nanowire composites for perovskite solar cells. *Nanoscale*. 2016;8(12):6308-6316.
29. Hu L, Wu H, Cui Y. Metal Nanogrids, Nanowires, and Nanofibers for transparent electrodes. *MRS Bulletin; Warrendale*. 2011;36(10):760-765.
30. Kumar MH, Yantara N, Dharani S, et al. Flexible, low-temperature, solution processed ZnO-based perovskite solid state solar cells. *Chem Commun*. 2013;49(94):11089-11091.
31. Liu D, Kelly TL. Perovskite solar cells with a planar heterojunction structure prepared using room-temperature solution processing techniques. *Nat Photon*. 2014;8(2):133-138.
32. Zhang Q, Dandeneau CS, Zhou X, Cao G. ZnO Nanostructures for dye-sensitized solar cells. *Adv Mater*. 2009;21(41):4087-4108.
33. Paranthaman MP, Wong-Ng W, Bhattacharya RN. *Semiconductor materials for solar photovoltaic cells.* Vol 218. 1st ed. 2016 ed. Cham: Springer; 2016.
34. Shockley W, Queisser HJ. Detailed balance limit of efficiency of p-n junction solar cells. *Journal of Applied Physics*. 1961;32(3):510-519.
35. ShockleyQueisserBreakdown2.svg. https://commons.wikimedia.org/wiki/File:ShockleyQueisserBreakdown2.svg
36. Best research-cell efficiencies. https://www.nrel.gov/PV/assets/images/efficiency-chart.png Web site. .
37. Leijtens T, Eperon GE, Noel NK, Habisreutinger SN, Petrozza A, Snaith HJ. Stability of metal halide perovskite solar cells. *Advanced Energy Materials*. 2015;5(20):n/a.
38. Matteocci F, Cinà L, Lamanna E, et al. Encapsulation for long-term stability enhancement of perovskite solar cells. *Nano-energy*. 2016;30:162-172.
39. Leijtens T, Eperon GE, Pathak S, Abate A, Lee MM, Snaith HJ. Overcoming ultraviolet light instability of sensitized $TiO_2$ with meso-superstructured organometal tri-halide perovskite solar cells. *Nature communications*. 2013;4:2885.
40. Sha WEI, Ren X, Chen L, Choy WCH. The efficiency limit of CH3NH3PbI3 perovskite solar cells. *Appl Phys Lett*. 2015;106(22):221104.
41. Xing G, Mathews N, Sun S, et al. Long-range balanced electron- and hole-transport lengths in organic-inorganic CH3NH3PbI3. *Science (New York, N.Y.)*. 2013;342(6156):344-347.
42. Manser JS, Kamat PV. Band filling with free charge carriers in organometal halide perovskites. *Nature Photonics*. 2014.
43. Conings B, Drijkoningen J, Gauquelin N, et al. Intrinsic thermal instability of methylammonium lead trihalide perovskite. *Advanced Energy Materials*. 2015;5(15):n/a.
44. Boix PP, Agarwala S, Koh TM, Mathews N, Mhaisalkar SG. Perovskite solar cells: Beyond methylammonium lead iodide. *The journal of physical chemistry letters*. 2015;6(5):898.
45. E. Eperon G, D. Stranks S, Menelaou C, B. Johnston M, M. Herz L, J. Snaith H. Formamidinium lead trihalide: A broadly tunable perovskite for efficient planar heterojunction solar cells. *Energy & Environmental Science*. 2014;7(3):982-988.
46. Jeon NJ, Noh JH, Yang WS, Kim YC, Ryu S, et al. Compositional engineering of perovskite materials for high-performance solar cells - ProQuest. *Nature*. 2015;517(7535).
47. Formamidinium iodide (FAI). Ossila Web site. https://www.ossila.com/products/formamidinium-iodide-fai.
48. Lee SJ, Pil Kim H, Mohd Yusoff, Abd Rashid bin, Jang J. Organic photovoltaic with PEDOT:PSS and V2O5 mixture as hole transport layer. *Solar Energy Materials and Solar Cells*. 2014;120(Part A):238-243.
49. Lattante S. Electronics. *Electronics*. 2014;3(1):132-164. http://www.mdpi.com/2079-9292/3/1/132.
50. Docampo P, Ball JM, Darwich M, Eperon GE, Snaith HJ. Efficient organometal trihalide perovskite planar-heterojunction solar cells on flexible polymer substrates. *Nature Communications*. 2013;4.
52. Peng Q, Tanaka S, Ito S, et al.  inorganic hole conductor-based lead halide perovskite solar cells with 12.4% conversion efficiency. *Nature Communications*. 2014.
53. Fantacci S, Angelis F, Nazeeruddin M, Grätzel M. Electronic and optical properties of the spiro-MeOTAD hole conductor in its neutral and oxidized forms: A DFT/TDDFT investigation. *The Journal of Physical Chemistry C*. 2011;115:23126–23133.
54. Poly(3-<WBR>hexylthiophene-<WBR>2,5-<WBR>diyl) 445703. Sigma-Aldrich Web site. https://www.sigmaaldrich.com/catalog/product/aldrich/445703.
55. Wijeyasinghe N, Anthopoulos TD. Copper(I) thiocyanate (CuSCN) as a hole-transport material for large-area opto/electronics. *Semicond Sci Technol*. 2015;30(10):104002.
56. Perera VPS, Senevirathna MKI, Pitigala, P K D D P, Tennakone K. Doping CuSCN films for enhancement of conductivity: Application in dye-sensitized solid-state solar cells. *Solar Energy Materials and Solar Cells*. 2005;86(3):443-450.

57. §, T X, Qinglong Jiang, Xia Sheng, Bing Shi, Xinjian Feng. Nickel-cathoded perovskite solar cells. . 2014.
58. Albrecht S, Rech B. Perovskite solar cells: On top of commercial photovoltaics. *Nature Energy*. 2017;2(1):16196.
59. Orr F. 2015 quadrennial technology review. *Proceedings of the International Conference for High Performance Computing, Networking, Storage and Analysis*. 2015.
60. Dorval Dion CA, Tavares JR. Photo-initiated chemical vapor deposition as a scalable particle functionalization technology (a practical review). *Powder Technol*. 2013;239:484-491.
61. Selvakumar N, Barshilia HC. Review of physical vapor deposited (PVD) spectrally selective coatings for mid- and high-temperature solar thermal applications. *Solar Energy Materials and Solar Cells*. 2012;98(Supplement C):1-23.
62. Nie W, Tsai H, Asadpour R, et al. High-efficiency solution-processed perovskite solar cells with millimeter-scale grains. *Science*. 2015;347(6221):522-525.
63. Xiong K, Hou L, Wu M, et al. From spin coating to doctor blading: A systematic study on the photovoltaic performance of an isoindigo-based polymer. *Solar Energy Mater Solar Cells*. 2015;132:252-259.
64. Lin Y, Cai C, Zhang Y, et al. Study of ITO-free roll-to-roll compatible polymer solar cells using the one-step doctor blading technique. *J.Mater.Chem.A*. 2017;5(8):4093-4102.
65. Fabrication and characterization of zinc oxide (ZnO) Nanoparticle by sol-gel method. .
66. Scriven LE. Physics and applications of DIP coating and spin coating. *MRS Online Proceedings Library Archive*. 1988;121.
67. Huang F, Dkhissi Y, Huang W, et al. Gas-assisted preparation of lead iodide perovskite films consisting of a monolayer of single crystalline grains for high efficiency planar solar cells. *Nano-energy*. 2014;10(Supplement C):10-18.
68. Kim BJ, Kim DH, Lee Y, et al. Highly efficient and bending durable perovskite solar cells: Toward a wearable power source. *Energy Environ Sci*. 2014;8(3):916-921.
69. Chen Z, Cotterell B, Wang W, Guenther E, Chua S. A mechanical assessment of flexible optoelectronic devices. *Thin Solid Films*. 2001;394(1):201-205.
70. Martin Kaltenbrunner, Matthew S White, Eric D Glowacki, et al. Ultrathin and lightweight organic solar cells with high flexibility. *Nature Communications*. 2012;3:770.
71. Nickel F, Haas T, Wegner E, et al. Mechanically robust, ITO-free, 4.8% efficient, all-solution processed organic solar cells on flexible PET foil. *Solar Energy Materials and Solar Cells*. 2014;130:317-321.
72. Dupont SR, Oliver M, Krebs FC, Dauskardt RH. Interlayer adhesion in roll-to-roll processed flexible inverted polymer solar cells. *Solar Energy Materials and Solar Cells*. 2012;97:171-175.
73. Zhao Y, Nardes AM, Zhu K. Solid-state mesostructured perovskite CH3NH3PbI3 solar cells: Charge transport, recombination, and diffusion length. *J Phys Chem Lett*. 2014;5(3):490-494.
74. Yaacobi-Gross N, Treat ND, Pattanasattayavong P, et al. High-Efficiency organic photovoltaic cells based on the Solution-Processable hole transporting interlayer copper thiocyanate (CuSCN) as a replacement for PEDOT:PSS. *Advanced Energy Materials*. 2015;5(3):n/a.

# 10.0 Appendix A: Layer Processing Procedures

The final layer processing procedures of our solar cells made during the project. All layers procedures were the same if done one ITO-PET, PET, and ITO-glass. The procedures specify concentrations of solutions, exact procedures for solution processing, and exact procedures for layer coating techniques.

## 10.1 Substrate Etching and Cleaning Procedure

This procedure is applicable for FTO Glass, ITO glass, and ITO PET substrates. The cutting procedures are subject to the starting glass or plastic size.

<u>Cutting glass slides in the sample squares:</u>

1. Draw guidelines on the sample to cut 20mm x 25 mm squares or 15mm x 25mm squares.
2. Use the diamond stylus to scratch a line on the sample.
    a. Use a ruler or other straight edge to guide the diamond stylus.
3. Use the clamp with the white stripe under the crack (facing down), just using the tip of the clamp on the edge of the sample, to crack it along the line.
4. Repeat step three to separate all samples.

<u>Cutting plastic (PET) slides in the sample squares:</u>

1. Draw guidelines on the sample to cut 20mm x 25 mm squares or 15mm x 25mm squares.
2. Use scissors to cut the plastic into squares.
3. Repeat step 2 until all sample squares are separated.

<u>Etching procedure:</u>

1. Determine which side has the ITO conductive film on it.
    a. Use multimeter to test resistance, one side should overload and the other will have close to the resistance of the ITO purchased.
    b. A second check can be done by using tweezers to scratch both sides gently, the side that feel rougher has the ITO, the smooth side is glass.
2. Tape the ITO side with Teflon tape so that a 2mm - 5mm strip of ITO is visible and the rest is covered by tape.
3. Press out any bubbles that you can, making sure the edges of the tape will not allow any liquid under.
    a. A flat edge such as a razor blade cane be used to flatten the tape.
4. Cut the ends of the tape close to flush and wrap the small leftover tape around the glass square.
5. Repeat steps 1-4 for as many samples as desired.

6. Place tape covered ITO into a glass Petri dish and place under the fume hood.
7. Using a metal spudger take small amounts of zinc powder and spread it on the uncovered parts of the ITO.
8. Pipet 1mL of 6 molar HCL slowly dropwise onto the Zinc and exposed ITO, making sure not to touch the pipet to the sample.
9. Add HCl as necessary to fully react the zinc.
10. Wait for a few minutes until the bubbles stop.
11. Rinse the sample in the petri dish with the DW (Deionized water) in the fume hood.
12. Pour out the liquid mixture into the correct disposal bottle labeled with Zinc DW and HCL
13. Repeat steps 11-12 two to three times to clean the sample.

Cleaning Procedure:

1. Next fill the petri dish to just above the sample with 1:1:1 $H_2O$+Acetone+Isopropanol.
2. Wash the samples by hand and place the petri dish floating in the sample vibrator, set it to five minutes and run the sonic mode.
3. Repeat step 2 three times.
4. Place the waste into the matching Acetone container in the back left of the fume hood.
5. Finally using the 1 mL pipet deposit 1-Propanol spectrophotometric grade onto the sample, repeating until just barely above the sample in the petri dish.
6. Place in the sonic cleaner for 20 minutes.
7. Take the glass squares out individually with a pair of tweezers and blow air on the squares to dry and let sit in fume hood until visible dry.
8. Place them in a petri dish to store.

## 10.2 Zinc Oxide Nanoparticle Layer Procedure

<u>Solution processing:</u>

1. Make 125 mL methanol solution in a beaker using the beaker to roughly measure volume and dissolve Zinc acetate dihydrate (2.9 g, 13.4 mmol) in it.
2. Set a hotplate in the fume hood for 155C to bring the temperature of the solution to 65 C. Monitor solution temperature with an alcohol thermometer. Solution should be "boiling" if at 63-65C. Keep the solution covered as much as possible.
3. Make KOH (1.48 g, 23 mmol) in methanol (65 ml) in a beaker and stir until dissolved.
4. Place KOH solution in a titrator mounted above the Zinc acetate dihydrate beaker.
5. Add KOH solution to Zinc solution dropwise in a titrator over a 15 min period with the Zinc solution heated and stirred at 60C - 65C.
    a. Titration rate should be about 3 drops per second.
6. Stir the reaction mixture for 2.5 h at 65 C on hot plate while covered with parafilm.
7. Turn off hot plate and allow to cool to room temperature (0.5 - 1 hour), the solution should separate visibly with a solvent layer on top.
8. Clean a glass stir rod in methanol.
9. Pour the contents equally into 4 centrifuge vials.
10. Centrifuge for 5 min to separate precipitate from methanol.
11. Decant the solvent into a waste bottle.
12. Repeat steps 9-11 as many times as necessary to have all the solution in the four vials from the beaker.
13. Add 3-5 mL of methanol to each vial while keeping the solution levels equal for each vial.
14. With the glass stir rod, mix the Nanoparticles and solvent.
15. Centrifuge for 5 min to separate precipitate from methanol.
16. Repeat steps 13-15 two times to wash the ZnO.
17. Add n-butanol (70 ml), methanol (5 ml) and chloroform (5 ml) in a new beaker.
18. Add 10 mL of solution made in step 17 to each vial and physically disperse by using the stir rod.
19. Dump solution back into beaker.
20. Stir solution to disperse particles or use sonication.
21. Prepare a second beaker of equal size by cleaning with acetone.
22. Use 100mm diameter, 20-25um filter paper, fold to make a conular shape. Pour unfiltered ZnO slowly through the filter paper until the solution has been completely moved into the new beaker.
23. Before spin coating, filter the ZnO solution one last time with a .45um filter.

** All temperatures should be monitored with a thermometer in solution; the hot plate will be much hotter than 65C, about 155C - 185C

Spin coating procedure:

1. Disperse particles by sonication or stirring at least 5 minutes.
2. Set program on spin coater to 3000 RPM, 30 S, 1000.
3. Make sure the surface is right side up by testing for the resistance of ITO.
4. Clean Spin coater pedestal with Acetone.
5. Place Sample on Spin coater.
6. Use a pipet to drop 100-200 microliters on the sample (enough to fully cover, do not overflow).
7. Run program.
8. Repeat steps 6-7 five times.
9. After spin coating is finished, remove the sample by disabling the vacuum.
10. Wipe back of sample if dirty or has marks from the spin coater.
11. Let samples dry for 2 min in fume hood.

Notes:

- It is best to do 0.45um filter close to spin coating so the solution is not allowed to conglomerate.
- The syringes used for the last filter step are very finicky and not meant to be used more than once, they can jam and a full solution can take 6-8 syringes to complete and a lot of squeezing power, wear safety goggles at all times because solution can splatter.
- This amount of solution can make about 30 samples.
- Solution lasts for 2 weeks.
- Solution concentration is about 6 mg/mL.

## 10.3 Methylammonium Lead Iodide Layer Procedure

Solution Processing:

1. Weigh 0.460g of PbI2, add it to a vial and dissolve with 1 mL solution of DMF.
2. Stir the solution on a hot plate for 70C for 10 min or until a uniform yellow solution is created.
3. Create a second solution of MAI/2-Propanol at a concentration of 10mg/mL to make 25 mL of total solution.
4. Before spin coating, filter PbI2 solution with a 0.45 um filter.

*Will make 4-5 samples

Spin coating and dipping procedure:

1. Heat solution at 70C.
2. Set program on spin coater to 3000 RPM, 15 S, 1000 RPM/s.
3. Make sure the surface is right side up by testing for the resistance of ITO.
4. Place Sample on Spin coater.
5. Use a pipet to drop 100-200 microliters on the sample (enough to fully cover).
6. Run program.
7. After spin coating is finished, remove the sample by disabling the vacuum.
8. Hold sample with tweezers at the end where the sample will be cleaned to leave bare ITO, dip the sample vertically in MAI/2-Propanol solution for 1 min without touching the tweezers in the solution.
9. Lightly clean of back of sample and lightly spray compressed air to dry the sample.

## 10.4 Copper Thiocyanate Layer Procedure

Solution concentration is 40mg/mL CuSCN in diethyl sulfide

<u>Solution processing:</u>

1. Place wax paper on the scale and zero the scale.
2. Measure out 40 mg of CuSCN with a spudger cleaned with acetone.
3. Place the 40 mg into a small vial carefully.
4. Add a Stirrer cleaned with acetone and place in the vial.
5. Add 1mL of diethyl sulfide, 98% concentration, to a scintillation vial.
6. Use the sonic vibrator plate to stir the solution in the vial for 24 hours.

<u>Spin coating:</u>

1. Set Hot plate to 65C.
2. Set program on spin coater to:
    a. 500 RPM, 60 S, 100 RPM/s.
    b. 5000 RPM, 30s, 1600 RPM/s.
3. Make sure the sample surface is right side up, the perovskite brown/black layer should look like it's on top, the bottom of the sample will look like it has a dark gloss finish.
4. Place Sample on Spin coater.
5. Use a pipet to drop 100-200 microliters on the sample.
6. Run program.
7. After spin coating is finished, remove the sample by disabling the vacuum.
8. Place sample covered on a hot plate for 10 min at 65 C.

*Will cover 4-5 samples

## 10.5 Poly(3-hexylthiophene-2,5-diyl) Layer Procedure

Solution concentration is 15mg/mL P3HT in 1,2 dichlorobenzene

<u>Solution processing:</u>

1. Place wax paper on the scale and zero the scale.
2. Measure out 15 mg of P3HT with a spudger cleaned with acetone.
3. Place the 15 mg into a small vial carefully.
4. Add a Stirrer cleaned with acetone and place in the vial.
5. Add 1mL of dichlorobenzene to a scintillation vial.
6. Set hot plate to 60C.
7. Stir and heat solution until all black P3HT dissolves and a orange/red solution is made.

<u>Spin coating:</u>

1. Set program on spin coater to 2000 RPM, 20s, and 600 RPM/s.
2. Make sure the sample surface is right side up, the perovskite brown/black layer should look like it's on top, the bottom of the sample will look like it has a dark gloss finish.
3. Place sample on spin coater.
4. Use a pipet to drop 100-200 microliters on the sample.
5. Run program.
6. After spin coating is finished, remove the sample by disabling the vacuum.
7. Let the sample dry for 30s.

*Will cover 4-5 samples

# 11.0 Appendix B: Testing Procedures

During the final stages of our project, we tested our samples in two flexibility methods and the power conversion efficiency of the completed cells. Each of these procedures is outlined in detail below.

## 11.1 Flexibility Testing Procedure

This sample method applies to PET samples, Kapton samples, and staircase samples. The Observational Testing was only used for the PET samples.

Procedure Setup

1. Prepare the samples by designating two sides of the cell that can be taped.
2. If the cell has imperfections pick the worst side as the tape will seriously damage the below layers.
3. Apply one piece of tape and leave that with a stick tab, maybe 3mm of tape attached to the top of the cell and the rest hanging off as a sticky tab, this will be used between objects.
4. Attach another tab in a similar manner on the other side.
5. For the large radius objects the cell will be placed on them then bent to be flush with the outside.
6. After each bend a resistance measurement will be conducted, these processes are outlined below.
7. Once the object circumference is smaller than the cell's length the cell is no longer bent around the object but rather the object rolls up the cell.
8. To do this remove the second tab that is usually held and tape the cell to the table edge, tape the other end to the object and roll it up maintaining the tension to assure the cell bends uniformly.
9. The cells being tested are bent at the largest radii first then the radii is reduced each subsequent time.
10. Observational and Quantifiable testing is to be completed either between each bend or it can be done before any bending and after it has been bent to the smallest radius.

Observational Testing

1. Between bending of the samples, they can be imaged using an optical microscope.
2. The sample must be at least 25x25mm otherwise it will in all likelihood fall through the optical microscope viewing platform.
3. Starting imaging at the lowest setting, baseline images should be taken at representative regions on the cell before bending.
4. Pick landmarks like scratches or visual imperfection that will remain on the cell during bending.

5. Zooming in on the cell can be helpful but realistically will probably not make any cracks more visual so it is not required to image as much as the low mag but can be good to verify cracking or lack thereof.
6. Repeat the imaging at the end of bending

Quantifiable Testing

1. Using the custom connection for the multimeter we are able to get repeatable resistance readings.
2. Attach the connector to the multimeter set to ohms by alligator clips.
3. The connector has prongs at a set distance apart so the readings are always the resistance of a surface over 1 cm.
4. Record the resistance before bending, depending on the amount of data being recorded test the sample in multiple areas and either record each individually or average the values.
5. Bend the sample and repeat the reading, when pressing the connector be sure to apply ample pressure without damaging the cell but maintaining the connection.

## 11.2 Power Conversion Efficiency Testing

Procedure Setup

1. Using the two stands and clamps on the table place the cell holder in front of the light source 130mm away from the end of the tube.
2. Position the holder so that it is 146mm tall, level with the source.
3. Place the cell into the holder so that the substrate for the sample is facing the light source and the contact points are facing away.
4. Three cables are connected to the potentiostat, the Blue wire connects to the black cable and the Red wire connects to the red.
5. Using a second set of stands affixed to two banana plug probes, position them so the Red is pressed against the ITO or bottom conductor on the cell and the Black is touching the top gold conductor very lightly.
6. Do not use too much pressure on the gold or you might damage the cell, be sure to connect it after the ITO so that you are less likely to scratch the cell.
7. Cover the lamp with tinfoil so that you aren't exposing the cell outside of testing.
8. Turn the lamp on and open up the program for the potentiostat.
9. Flick the switch on the blue box behind the monitor on, wait about 30 seconds to hear a click from the box then connect to the SP-200 Potentiostat in the program.
10. Load the profile of a similar cell or modify the parameters to fit the test best then click the run button.
11. This will bring up the option to save the file, as soon as you save it within whatever directory you want it will run, rename it what you will.
12. Right before you hit save remove the tinfoil and expose the cell, then save.
13. The same cell can be tested multiple times and the contact points can be adjusted if there are connectivity issues.
14. If possible covering portions of a sample can protect other cells from being too exposed while not being tested.
15. The data collected can be exported in a format readable by Excel which will allow the values to modified to accurately represent the PCE.

Modifying the data

1. Export the file data as an .mpr file.
2. Copy the Ewe/V and I/mA columns to a new file as column A and B.
3. Name Column C Ewe (V) and it's values are Column A*(-1).
4. Calculate the area of the cell by measuring the size of the gold conductor, get this area in cm.
5. Column D will be labeled I (mA) and is equal to column B/Area of cell.
6. Column E will then be the Power in milliwatts and is equal to Column C*Column D.
7. The best PCE is then the max value from column E and can be quickly found using Excel.
8. Graphing the Power on the Y axis and Ewe on the X axis will give the power curve of the cell and can visualize the max PCE and the short-circuit voltage of the cell.

# 12.0 Appendix C: Additional Data and Images

## 12.1 Additional Data

*Table 9. Chemical List*

| **Layer** | **Product Name** | **CAS Number** | **Part Number** | **Manufacturer** | **Product Details** |
|---|---|---|---|---|---|
| ITO coated PET | ITO coated PET | N/A | 639303-1EA | Sigma-Aldrich | Surface Resistivity - 60Ω/sq, Transmittance - 550 nm, 79%, Radius of Curvature - 75mm, and thickness 1300 Å |
| ITO coated glass | ITO coated Glass | N/A | | SPI Supplies | Surface Resistivity 8-12Ω/sq, thickness 1.1mm |
| ZnO Nanoparticles | Zinc Acetate Dihydrate | 5970-45-6 | Z0625 | Sigma-Aldrich | |
| | Potassium hydroxide | 1310-58-3 | 1050321000 | Sigma-Aldrich | |
| | n-Butanol | 71-36-3 | W2171816 | Sigma-Aldrich | Flashpoint - 28.9C |
| | Methanol | 67-56-1 | | WPI Stockroom | Flashpoint 11.1C |
| | Chloroform | 67-68-3 | C2432 | Sigma-Aldrich | |
| $MAPbI_3$ | Lead Iodide | 10101-63-0 | 211168 | Sigma-Aldrich | |
| | N-Dimethylforamide anhydrous, 99.8% | 68-12-2 | 227056-100ML | Sigma-Aldrich | |
| | Methylammonium Lead Iodide (Liquid) | N/A | 808431-50mL | Sigma-Aldrich | Concentration - 0.42 M, in 2-propanol |
| | Methylammonium Lead Iodide (Powder) | 14965-49-2 | 793493-5G | Sigma-Aldrich | Melting point 270 - 280C |

| | | | | | |
|---|---|---|---|---|---|
| | 2-Propanol anhydrous, 99.5% | 67-63-0 | 278475-1L | Sigma-Aldrich | |
| CuSCN | Copper Thiocyanate, 99% | 1111-67-7 | 298212-50G | WPI Nano-energy Lab | |
| | Diethyl Sulfide, 98% | 352-93-2 | 107247-100ML | WPI Nano-energy Lab | |
| P3HT | P3HT | 156074-98-5 | | WPI Nano-energy Lab | Melting point 238C |
| | 1,2 Dichlorobenzene anhydrous, 99% | 95-50-1 | 240664-100ML | WPI Nano-energy Lab | |

*Table 10. Power Conversion Efficiency Data*

| Name | HTL | Short-circuit Current | Open Circuit Voltage | PCE (%) |
|---|---|---|---|---|
| GF180228A | P3HT | 4.7162 | 0.1816 | 0.2158 |
| GF180228B | P3HT | 3.3684 | 0.0943 | 0.0799 |
| GF180228C | P3HT | 0.2784 | 0.0052 | 0.0003 |
| GF180315A | CuSCN (500) | 0.0581 | 0.0010 | 0 |
| GF180315B | CuSCN (5000) | 0.4062 | 0.0111 | 0.0011 |
| GF180315C | P3HT | 2.2610 | 0.0474 | 0.0268 |

*Table 11. Flexibility Testing PET Samples*

| Sample | No bend | 57.8 (mm) | 45.9 (mm) | 31.2 (mm) | 26.5 (mm) | 12.4 (mm) | 5.0 (mm) | 3.8 (mm) | crease |
|---|---|---|---|---|---|---|---|---|---|
| P3HT | 1.8Ω | 1.8 | 1.8 | 1.8 | 1.9 | 1.7 | 1.9 | 1.8 | 1.7 |
| CuSCN 500 | 1.8Ω | 1.7 | 1.8 | 1.7 | 1.8 | 1.8 | 1.8 | 1.7 | 1.8 |
| CuSCN 5000 | 1.5Ω | 1.4 | 1.4 | 1.4 | 1.4 | 1.4 | 1.3 | 1.3 | 1.6 |
| Gold | 1.9Ω | 2.5 | 2.6 | 2.8 | 2.8 | 2.6 | 2.7 | 2.5 | 2.7 |
| ITO | 104 +/- 4Ω | 103 +/-4 | 105 +/-4 | 97 +/-8 | 109 +/- 10 | 124 +/- 15 | 127 +/- 15 | 1350 +/- 200 | 5730 +/- 300 |

*Table 12. Flexibility Testing Kapton Samples*

| Sample | No Bend | 12.4 (mm) | 10.1 (mm) | 4.0 (mm) | 2.6 (mm) | 0.9 (mm) | Crease |
|---|---|---|---|---|---|---|---|
| CuSCN 5000 | 1.6Ω | 1.6 | 1.4 | 1.6 | 1.6 | 1.5 | 1.4 |
| CuSCN 5000 | 1.6Ω | 1.5 | 1.5 | 1.6 | 1.5 | 1.5 | 1.5 |
| CuSCN 500 | 1.4Ω | 1.4 | 1.5 | 1.4 | 1.7 | 1.5 | 1.6 |
| CuSCN 500 | 1.4Ω | 1.4 | 1.4 | 1.6 | 1.5 | 1.5 | 1.6 |
| P3HT | 1.4Ω | 1.4 | 1.4 | 1.7 | 1.3 | 1.3 | 1.3 |
| P3HT | 1.4Ω | 1.4 | 1.4 | 1.3 | 1.5 | 1.4 | 1.2 |
| Gold | 1.2Ω | 1.3 | 1.2 | 1.2 | 1.4 | 1.4 | 1.3 |
| Gold | 1.3Ω | 1.2 | 1.2 | 1.5 | 1.5 | 1.3 | |

*Table 13. Flexibility Testing Staircase Samples*

| Sample | Region | No bend | 57.8 (mm) | 45.9 (mm) | 31.2 (mm) | 26.5 (mm) | 12.4 (mm) | 5.0 (mm) | 3.8 (mm) | crease |
|---|---|---|---|---|---|---|---|---|---|---|
| B | ITO/ITO | 160 +/- 3 Ω | 180 +/- 5 | 140 +/- 8 | 145 +/- 8 | 240 +/- 10 | 240 +/- 20 | 190 +/- 15 | 160 +/- 5 | 240 +/- 10 |
|  | Gold/ Gold | 2.6Ω | 2.5 +/- .1 | 2.4 | 2.5 | 2.5 | 2.8 +/- .1 | 2.8 | 2.0 +/- .1 | 60 +/- 10 |
|  | Gold/ ITO | 150 +/- 20Ω | 160 +/- 30 | 150 +/- 30 | 140 +/- 20 | 170 +/- 10 | 90 +/- 15 |  | 900 +/- 100 | 2500 +/- 100 |
| D | ITO/ITO | 230 +/- 5Ω | 240 +/- 5 | 270 +/- 5 | 290 +/- 5 | 290 +/- 10 | 285 +/- 15 | 290 +/- 5 | 340 +/- 10 | 360 +/- 50 |
|  | Gold/ Gold | 2.2 +/- .1Ω | 2.5 | 2.4 +/- .2 | 2.7 +/- .1 | 2.7 +/- .1 | 2.5 +/- .2 | 2.6 +/- .2 | 2.8 +/- .1 | 2.5 +/- 1 |
|  | Gold/ ITO | 75 +/- 10Ω | 72 +/- 5 | 75 +/- 5 | 70 +/- 8 | 80 +/- 5 | 85 +/- 5 | 87 +/- 3 | 890 +/- 40 | 1300 +/- 100 |
| F | ITO/ITO | 210 +/- 10Ω | 240 +/- 20 | 230 +/- 5 | 235 +/- 5 | 240 +/- 15 | 250 +/- 10 | 240 +/- 10 | 370 +/- 10 | 340 +/- 30 |
|  | Gold/ Gold | 2.4 +/- .2Ω | 2.5 +/- .2 | 2.5 +/- .1 | 2.3 +/- .1 | 2.2 +/- .1 | 2.2 +/- .2 | 2.5 +/- .2 | 2.2 +/- .2 | 4.3 +/- 0.5 |
|  | Gold/ ITO | 105 +/- 5Ω | 100 +/- 15 | 95 +/- 10 | 100 +/- 10 | 95 +/- 5 | 110 +/- 10 | 115 +/- 15 | 1300 +/- 100 | 2400 +/- 100 |

## 12.2 Solar Cell Diagrams

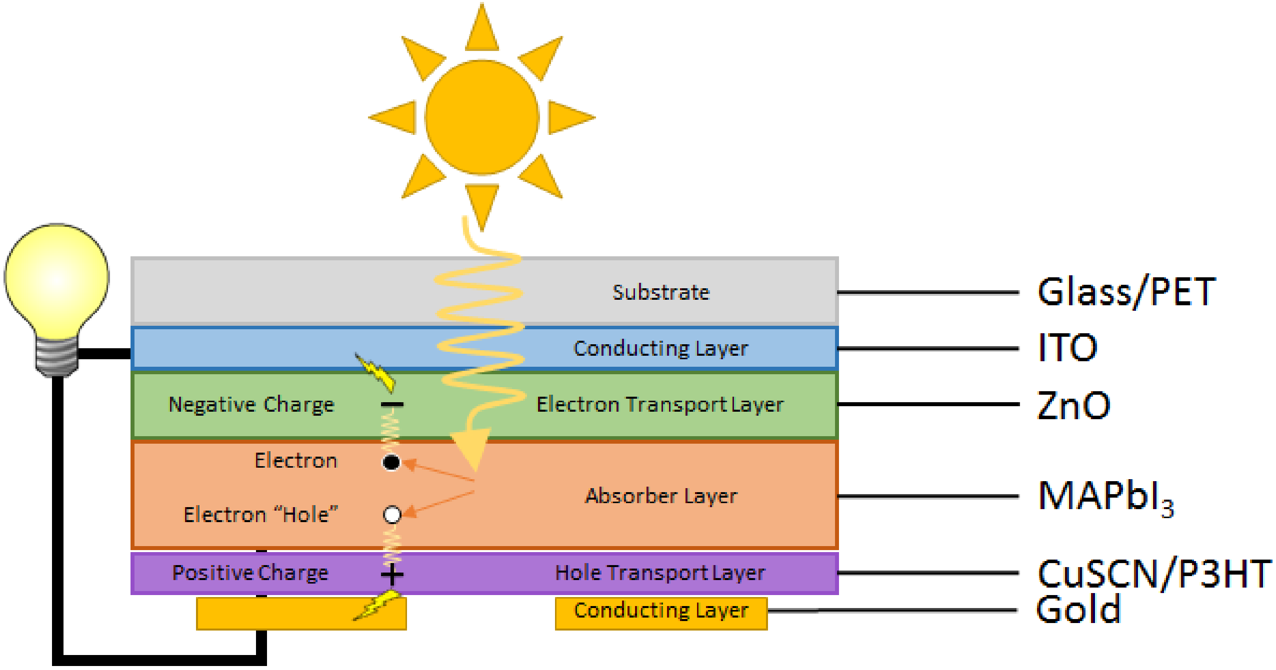

*Figure 38. Diagram of the electron movement in a solar cell.*

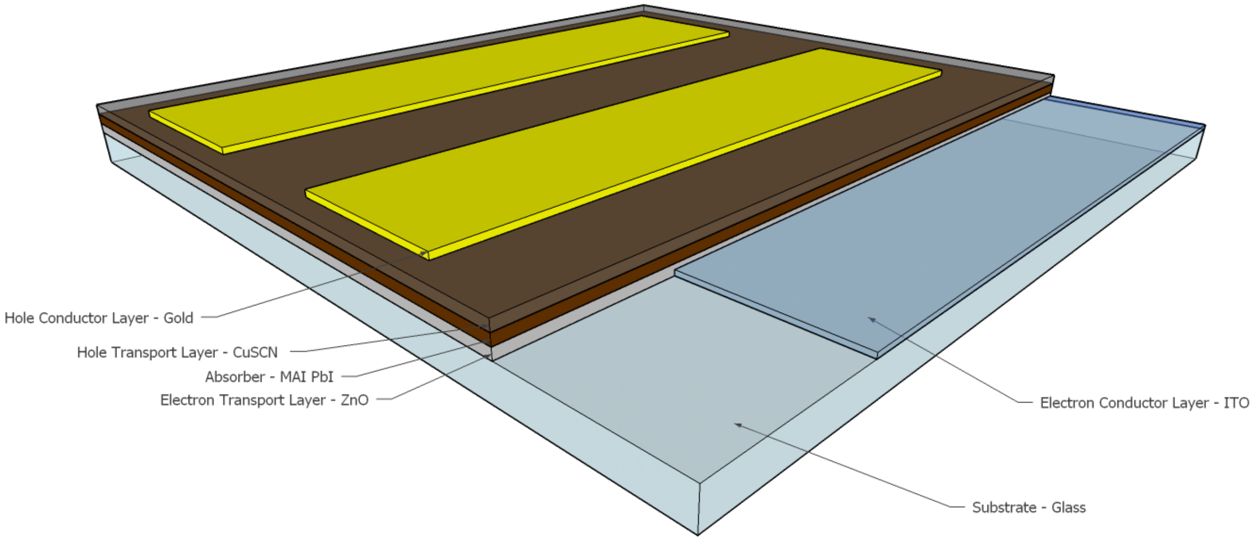

*Figure 39. A model of the solar cells made in the Nano-energy lab by our MQP group.*

## 12.3 Additional Optical Images

All images were taken at 20x magnification and the creased images were bent flat with a radius of curvature of 0.15mm.

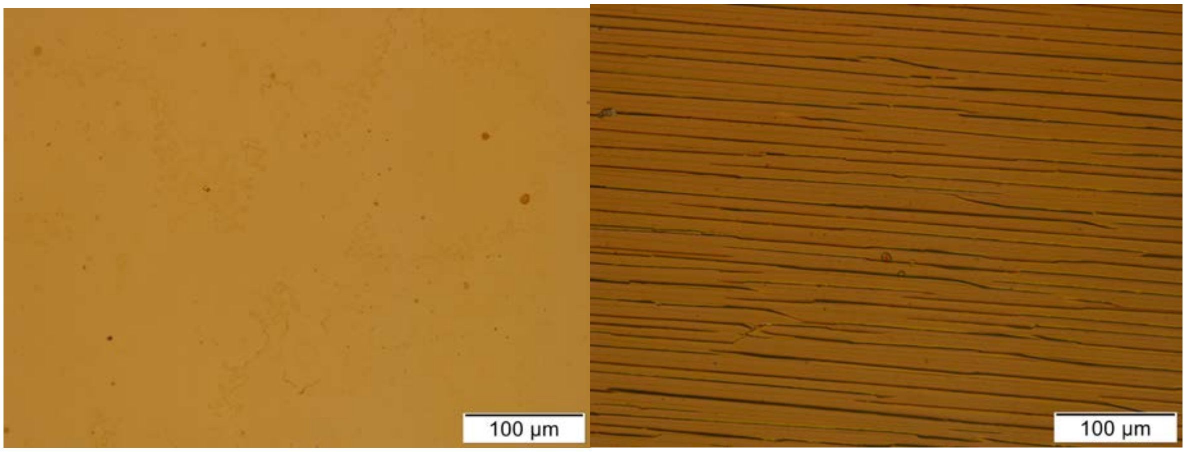

*Figure 40. (Left) unbent ITO PET (Right) bent ITO PET.*

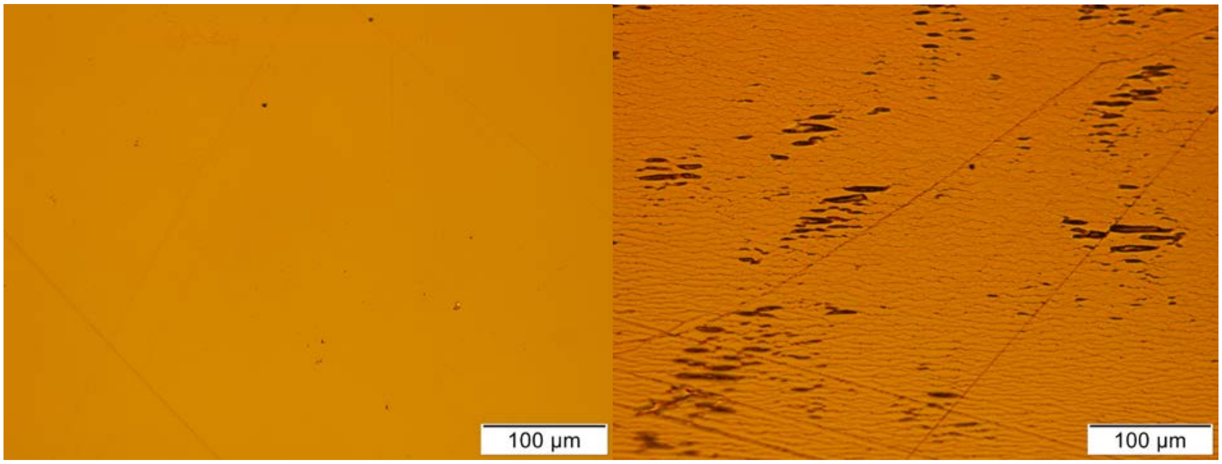

*Figure 41. (Left) Sample of gold on PET before bending (Right) Same Sample after crease bending.*

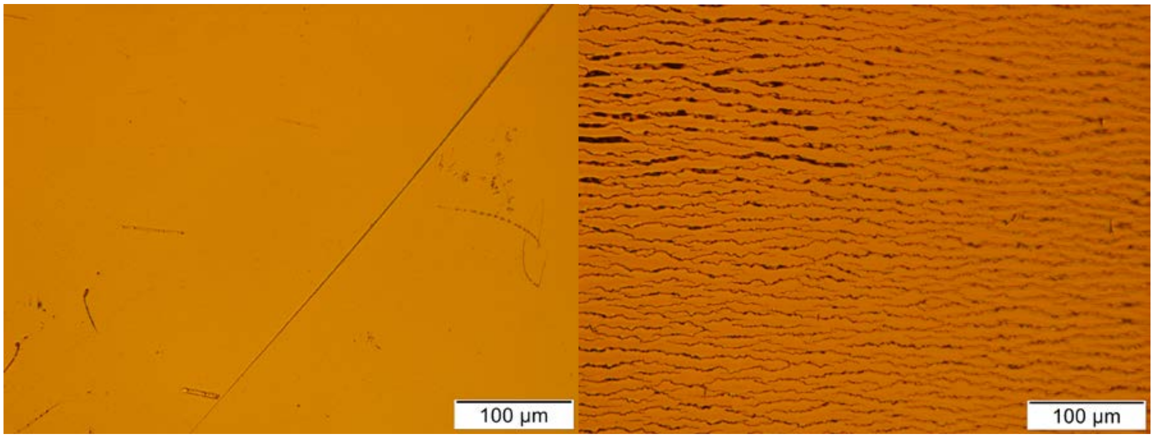

*Figure 42. (Left) Sample of gold and P3HT on PET before bending (Right) Same sample after crease bending.*

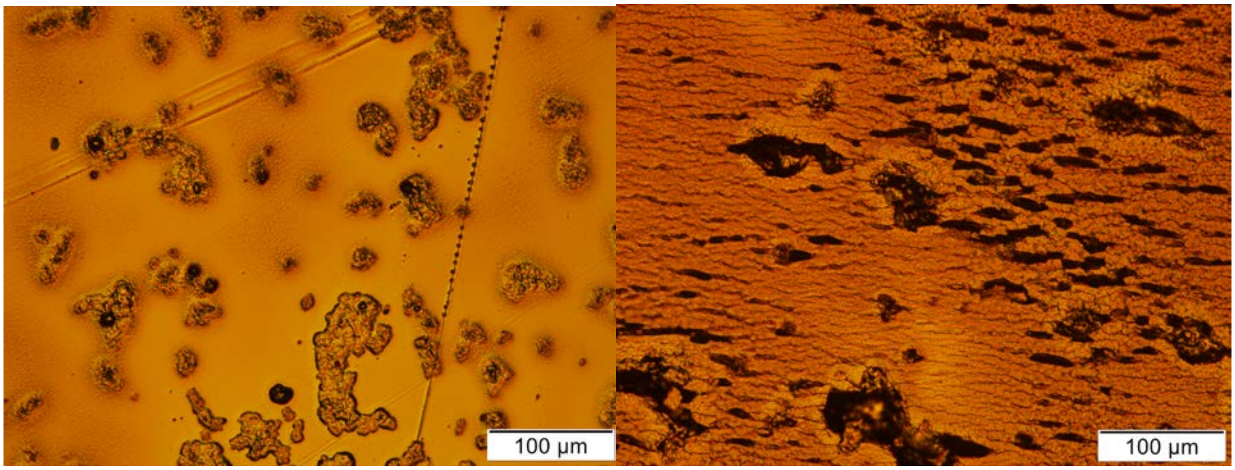

*Figure 43. (Left) Sample of gold and CuSCN 500 on PET before bending. (Right) Same sample after crease bending.*

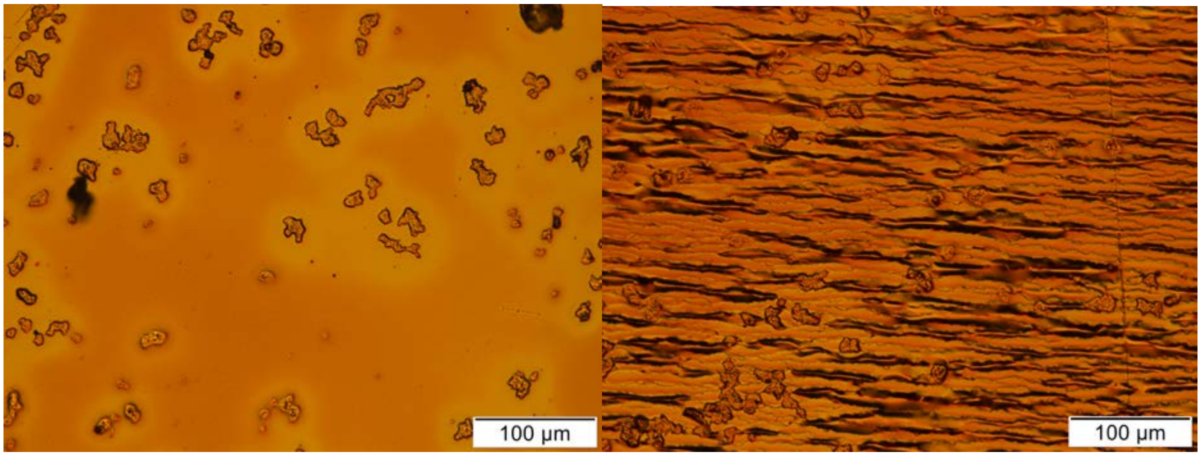

*Figure 44. (Right) Sample of gold and CuSCN 5000 on PET before bending. (Right) Same sample after crease bending (right).*

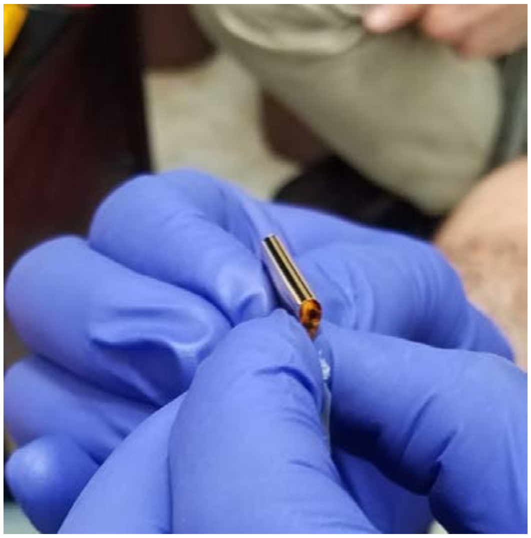

*Figure 45. Example of crease bending.*

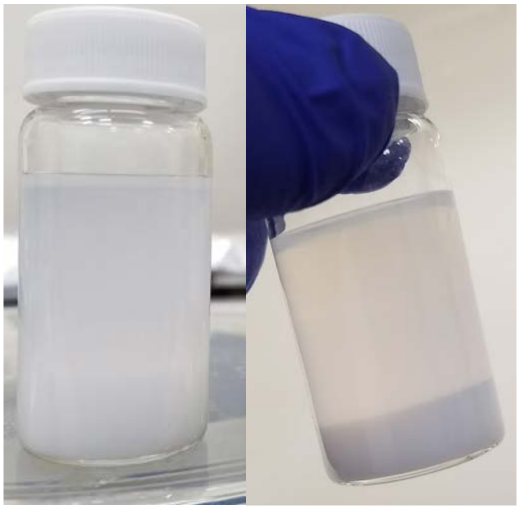

*Figure 46. (Left) ZnO solution after the initial 25µm filter. (Right) Same solution after sitting in the hood for 2 days.*

*Figure 47. Second set of solar cells before gold evaporation.*

*Figure 48. Working in the glovebox to apply the $MAPbI_3$ layer.*

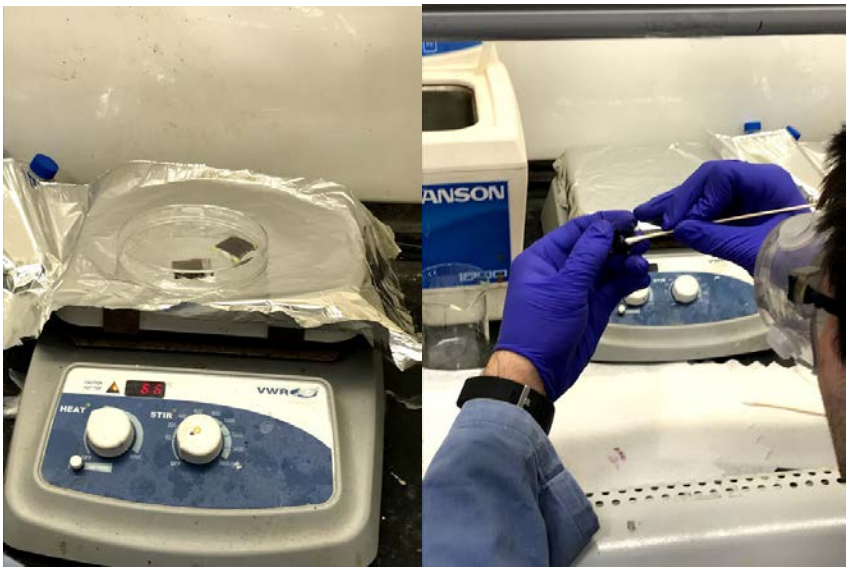

*Figure 49. Solar cell processing in the fume hood of annealing CuSCN and wiping the contact for the ITO conductor.*

## 12.4 SEM images

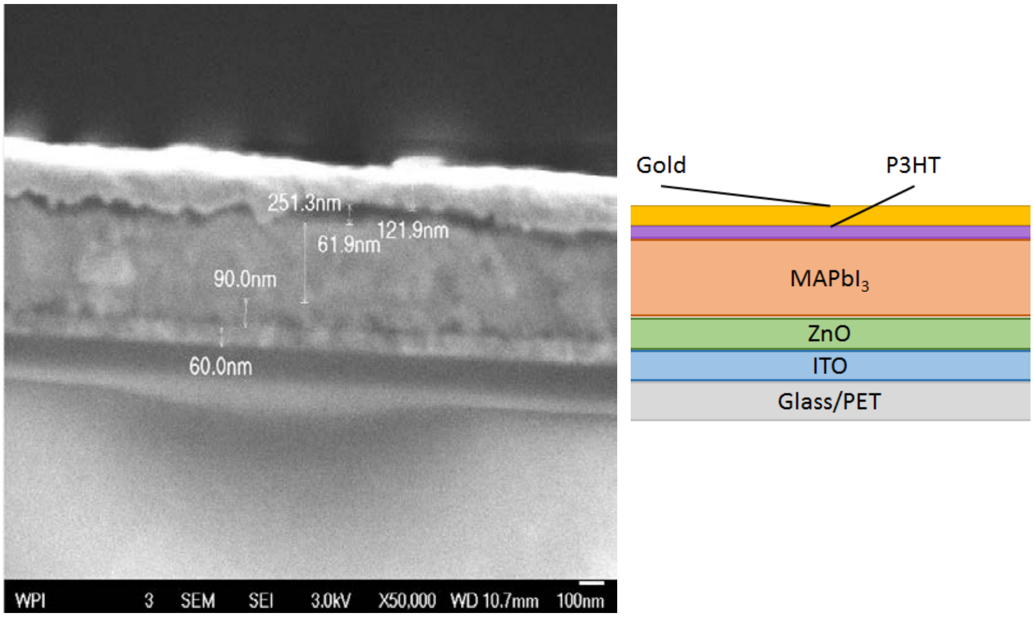

*Figure 50. This figure shows a layer comparison to the SEM image of a P3HT solar cell to a diagram to identify the layers in the solar cell.*

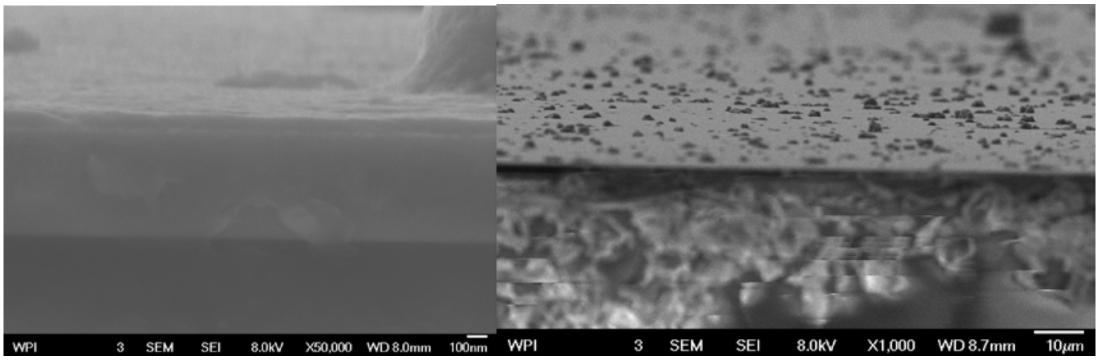

*Figure 51. Coating sample of ZnO filtered with a 25 μm filter.*